INVESTIGATION OF THE EFFECT OF DIFFERENT IONIC LIQUIDS ON THE CAPACITIVE PERFORMANCE OF BIOMASS DERIVED ACTIVATED CARBON

by

Maharun Negar Mojumder

A THESIS SUBMITTED IN PARTIAL FULFILLMENT OF THE REQUIREMENT FOR THE DEGREE

OF

MASTER OF SCIENCE IN CHEMISTRY

Department of Chemistry

BANGLADESH UNIVERSITY OF ENGINEERING AND TECHNOLOGY(BUET) DHAKA-1000, BANGLADESH.

February 2022

CANDIDATE'S DECLARATION

It is hereby declared that this thesis or any part of it has not been submitted elsewhere for the award of any degree or diploma.

Maharun

…..……………………

(Maharun Negar Mojumder)

Bangladesh University of Engineering and Technology (BUET), Dhaka-1000
Department of Chemistry

Certification of Thesis

A thesis on

INVESTIGATION OF THE EFFECT OF DIFFERENT IONIC LIQUIDS ON THE CAPACITIVE PERFORMANCE OF BIOMASS DERIVED ACTIVATED CARBON

By

Maharun Negar Mojumder

Roll No.: 1018032704, Session: **October-2018**, has been accepted as satisfactory in partial fulfillment of the requirements for the degree of Master of Science (M.Sc.) in Chemistry and certify that the student has demonstrated satisfactory knowledge of the field covered by this thesis in an oral examination held on February 23, 2022

Board of Examiners

1. Dr. Chanchal Kumar Roy
Assistant Professor
Department of Chemistry
BUET, Dhaka-1000.

Supervisor & Chairman

2. Dr. Md. Abdur Rashid
Professor and Head
Department of Chemistry
BUET, Dhaka-1000

Member (Ex-officio)

3. Dr. Al-Nakib Chowdhury
Professor
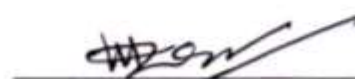Department of Chemistry
BUET, Dhaka-1000

Member

4. Dr. Ayesha Sharmin
Associate Professor
Department of Chemistry
BUET, Dhaka-1000

Member

5. Dr. Md. Mominul Islam
Professor
Department of Chemistry
University of Dhaka, Dhaka -1000

Member (External)

DEDICATED TO

MY FAMILY MEMBERS

AND

REVERENT TEACHERS

Acknowledgement

February 23, 2022

Maharun

....

(Maharun Negar Mojumder)

Abstract

Stable ionic liquids (ILs) are promising materials for extending the potential applications of electrolytes. Herein, the effects and capacitance performance of various ILs consisting of the same 1-butyl-3-methylimidazolium ([bmim]) cation and three different anions: bromide (Br^-), chloride(Cl^-), and hexafluorophosphate (PF_6^-) have been investigated with activated carbon (AC) derived from banana leaves for supercapacitor (SCs) applications. The specific capacitance (C_{sp}) values were obtained 177, 318, and 280 F g^{-1} in [bmim]Br, [bmim]Cl, [bmim]PF$_6$ electrolytes, respectively. The effect of the size of anions and polarizability has been found to affect the capacitance performance. In [bmim]Cl, the AC has obtained the best capacitance performance and rate capability. A comparison of electrochemical performance revealed that the electrolyte anions have a significant effect on the SCs efficiency. A mini-prototype device has been prepared to demonstrate the practicality of the AC and [bmim]Cl electrolytes. This study is expected to broaden the applications of ILs for SC devices

.

Table of Contents

List of Figures

List of Tables

Chapter-1
Introduction

1 Introduction

1.1 General Introduction

Supercapacitors (SCs), also known as electrochemical capacitors, are one of the most promising energy storage devices for meeting the power pulse-output demand of a variety of applications, including variable-speed wind turbines with improved reliability and efficiency, automated stacking and harbor cranes, and plane emergency systems during landing [1, 2]. The reasonable and smart energy solution is a new innovative resolve to ensure affordable and clean energy for all; goal no. 7 among the goals for SDG, 2030 set up by United Nations (UN) and meet the challenge of the 4th industrial revolution (4.0 IR) [3]. SCs are electrochemical double-layer capacitors (EDLCs) or pseudocapacitors, depending on the charge storage processes and active electrode materials utilized. On the other hand, Pseudocapacitors are based on the fast and reversible surface redox reaction of some conducting polymers[4]. EDLCs primarily use carbon-based materials with high surface area as active electrode materials [5-9], whereas pseudocapacitors rely on some conducting polymers and metal oxide fast and reversible surface redox reaction [10, 11]. The supercapacitor performance is dependent largely on the choice of electrolytes and electrode materials. The effective surface area is crucial in controlling the capacitive properties of the electrode; high capacitance and high energy density (E) without scarifying power density (P)[12]. Because E is related to capacitance and operating voltage, many studies first concentrated on increasing the electrode surface to increase EDL capacitance. Carbon nanomaterials such as carbon nanotubes (CNTs), activated carbon (AC) and graphene have been emphasized as materials with high capacitance [13, 14]. Biomass-based AC has attracted great attention as the efficient electrode material of electrochemical supercapacitors (ESCs) due to its advantages like unique hierarchical nanostructure, facile synthesis process, excellent electrical conductivity, and high specific surface area [15-17]. To increase total capacitance with pseudo-capacitance, materials for a redox-active electrode such as metal oxide and conductive polymer are proposed [18-20] . On the other hand, the active redox electrode has certain drawbacks,

including poorer electrical conductivity than carbonaceous electrodes, the inability to use the electrolyte in an aqueous environment, and a relatively limited life duration due to a partially irreversible chemical reaction. Widening the operating voltages is another way to increase E. In terms of improving E, raising the cell voltage would be more effective than increasing the electrode capacitance. This is since the E is proportional to the cell voltage squared. If the electrode materials are stable within the working voltage range, the operating cell voltage of the ESCs is primarily determined by the electrochemical stable potential window (ESPW) of the electrolytes[21]. So, the electrolyte is also an important component and significantly affects the performance of the supercapacitor. The electrolyte potential window and the interaction between the electrolyte and the electrode materials have a significant impact on the ES performance. The ionic conductivity of the electrolyte has a significant impact in the supercapacitor's internal resistance [22, 23]. To have a high capacitance and a high-P, the electrolyte ion size must be equal to or less than the pore size of the electrode material [23, 24]. The freezing point and viscosity of electrolytes impact the thermal stability of SC performance in a few circumstances, resulting in a shift in the operating voltage range [25, 26]. Apart from the operating voltage, the electrolytes have had a significant impact on other SCs performance metrics such as P, cycle stability, operating temperature, equivalent series resistance, lifespan, and self-discharge rate. Currently, numerous electrolytes have been produced and investigated based on the nature of the electrolyte, such as the ion type and size, ion concentration and solvent, ion-solvent interaction, electrolyte-electrode materials interaction, and potential window [27-30]. For instance, aqueous and organic-based electrolytes have been widely investigated in ECSs for biomass-based AC electrodes [22, 31-36]. It has been observed that a relatively narrow electrochemical potential window has restricted the practical applications of SCs in aqueous electrolytes [37]. Besides, commercially used organic electrolytes face safety issues for their volatility and flammable nature [25]. Ionic liquids (ILs) have recently shown promising prospects as electrolytes of SCs for their non-volatility, non-flammability, have a good thermal stability induced by negligible vapor pressure and wide electrochemical stable potential window [7, 29, 38, 39]. Additionally, ILs are solvent-free electrolytes that prevent the negative effect of solvation in the system[25]. Ions are usually solvated in bulk solutions but less when adsorbed at the electrode/electrolyte interface. The solvation effect must be considered when studying the link between pore size and specific capacitance (Csp) of porous carbons in aqueous

or organic electrolytes. Because ILs are exclusively composed of cations and anions, they have been employed in EDLC investigations to prevent the influence of solvation. Among these various ILs, ILs containing imidazolium cations are broadly studied due to their high ionic conductivities and relatively low viscosities [40, 41]. Despite these advantages, the SC system consisting of the biomass-AC and IL electrolyte has not been explored sufficiently for practical applications. For example, the variation of the chemical structure of the IL electrolyte on the performance of biomass AC has not been studied. To shed light on this, we will investigate the variation of anions of IL-based electrolytes with a fixed 1-butyl-3-methylimidazolium ([bmim]) cation structure on the ESC performance of biomass-based AC. Evaluation and comparison of performances of these SCs will advance the process of practical IL-based SCs

1.2 Objectives of the present work

The main objectives of this present work are to
  i.   synthesis of biomass-derived AC from banana leaves by chemical activation method
 ii.   chemical and morphological characterization of biomass-derived AC
iii.   evaluation of electrochemical performance of SCs from biomass-derived AC and different ILs
 iv.   correlate and comparison of the performance of the SCs.

1.3 Background

1.3.1 Overview of supercapacitor

SCs are energy storage devices with high E, P, and cycle life. They use an electrical double layer storage charge mechanism on the electrode-electrolyte interface and a pseudocapacitive mechanism on the surface and near-surface to bridge the gap between electrolytic capacitors and rechargeable batteries [21, 42, 43]. It's also known as gold capacitors, electrochemical capacitors, or ultracapacitors [44]. SCs can charge and discharge quickly due to the use of materials with a high surface area and porous and excellent conductive substances, resulting in a high-power delivery in a short period, resulting in their increased use in portable electronics, automobiles, buses, trains, cranes, and elevators due to their short charge-discharge time, which means required high P. SCs fill the gap between batteries, which can store more energy (high E), but

dispense it at a very slow rate, and regular electric capacitors have less energy but can release it extremely rapidly (high P) [45-47].

The main difference between SCs, batteries, and fuel cells is their charge storage techniques, which define their energy storage capacity. While SCs and batteries store charge in the electrode material, fuel cells are open systems that require a source of fuel (hydrogen or methanol) and an oxidant (oxygen or air) to function[47-48] .The life cycle of a fuel cell is substantially longer than that of a battery if a constant supply of fuel (hydrogen, methanol, or oxygen, depending on the type of fuel cell) is maintained. Due to their high energy storage capability, fuel cells are more attractive than batteries and find their use in interplanetary applications, which are still more expensive to manufacture. Due to a large amount of energy per unit weight or volume of batteries like Lithium-ion batteries (LiBs), we are getting much devotion in portable electronic markets and transportation applications. Despite the significant gains recorded on Li-ion batteries, they still face considerable hurdles in cycle life and maintaining thermodynamic stability due to chemical processes that occur on the electrode/electrolyte interphase in the battery. Researchers are currently concentrating on enhancing the electrode material for successful Li-ion intercalation and boosting the P while preserving the energy storage capacity to overcome these problems [48-50]. Long cycle life and fast charging are dependent on chemical energy stored mechanisms in the bulk of the electrode material, which is a limiting factor for increasing battery power. On the other hand, SCs store energy by charge separation and can be charged or discharged in seconds while having a long cycle life. The charge storage mechanism of SCs is mostly determined by the electrode materials. There are two types of SCs: electrical double-layer capacitors (EDLCs) and pseudocapacitors. For charge storage, the former relies on the electrical double layer on the electrode/electrolyte interface, whereas the latter depends on the surface or near-surface faradaic processes on the electrode-electrolyte contact [51]. SCs have a high P, but a poor E compared to batteries and fuel cells due to variations in their charge storage processes [21]. To overcome this challenge, it is necessary to develop a single energy storage device with both high energy and power densities, improve the E of ESCs to match those of lithium-ion batteries or combine both devices to produce hybrid energy storage devices to ensure power supply longevity. Now, most research is focused on boosting the energy storage capabilities of SCs while sacrificing little or no power capabilities by inventing

functional materials for electrode fabrication [21, 52].

1.3.2 Principles of energy storage mechanism of supercapacitor

The energy storage mechanisms of SCs can be classified into two types: electrochemical double-layer mechanisms based on electrostatic attraction, as in electrical double-layer capacitors, in which non-faradaic reactions occur, and pseudocapacitive behavior based on faradaic reactions, as in accumulators, and hybrid type electrodes based on a combination of the two [53].

➢ **Electrochemical double-layer capacitance**

The electrical energy is stored at the electrode/electrolyte interface by forming an electrical double layer in an EDLC (also known as the Helmholtz double-layer) because of reversible ion adsorption from the electrolyte onto the electrolyte active materials of electrodes with a high specific surface area [54]. The ions pass through the porous electrode when an electrode is immersed in an electrolyte. In contrast, charges on the electrode surface spontaneously rearrange themselves in a specific order and are accumulated in the double layer primarily due to electrostatic forces, with no phase transformation in the electrode materials. As a result, the maximum charge density is collected in the distance of the outer Helmholtz plane, i.e., at the centre of the electrostatically attracted solvated ions [55, 56].

Because of the large interfacial area and atomic range of charge separation distances, SCs can store much more energy based on EDL. In contrast, conventional capacitors store little energy due to the limited charge storage areas and geometric constraints of the separation distance between the two charged plates [57]. The electrode/electrolyte interface forms two layers of opposing charge separated by an atomic distance; according to Helmholtz, ions at the electrode/electrolyte interface are displaced and diffuse across the electrodes through the electrolyte. Consequently, an electrical double layer (approximately 5-10 mm thick) forms, with one layer on the electrode surface and the other in the electrolyte, as illustrated in Figure 1.3.2.1 [58]. In 1910, Gouy improved the Helmholtz model by including random thermal motion, which prompted him to assume a spatial distribution of ionic charge in the electrolyte to account for the voltage dependence of capacitance is today known as a diffused layer. Chapman developed a mathematical model of the diffused layer in 1913 to explain the ion distribution in the

electrolyte [55, 58].
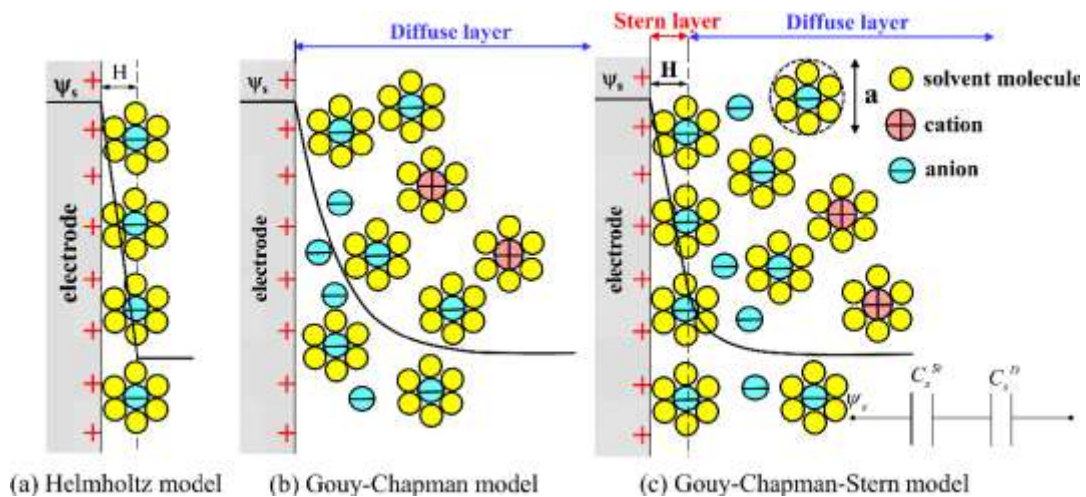
Figure 1.3.2.1 Schematic illustration of electrical double layer structures using the Helmholtz, Gouy-Chapman, and Gouy-Chapman-Stern models. H stands for the double-layer spacing and the Stern layer thickness in the Helmholtz model, whereas ψ_s stands for the potential at the electrode surface [58].

Gouy had previously thought that the ions were point charges, implying that point charge ions near the electrode surface would have a very large capacitance value. The Gouy-Chapman model, on the other hand, failed because of the same assumption, which resulted in an overestimation of the total capacitance of the electrodes due to an inaccurate potential profile [58]. Stern explained in 1924s a combined Helmholtz and Gouy–Chapman model that recognized two zones of ion distribution: the compact layer, also known as the Stern layer, and the diffuse layer (as shown in Figure 1.3.2.1). The electrode heavily absorbs ions (frequently hydrated) in the compact layer. In addition, the compact layer consists of specifically adsorbed ions (in most cases, they are anions irrespective of the charged nature of the electrode) and non-specifically adsorbed counterions.

The inner Helmholtz plane (IHP) and outer Helmholtz plane (OHP) are used to distinguish the two types of adsorbed ions. The diffuse layer region is what the Gouy–Chapman model defines[58]. The capacitance in the EDL (C_{dl}) can be treated as a combination of the capacitances from two regions, the Stern type of compact double layer capacitance (C_H) and the diffusion region capacitance (C_{diff}). Thus, C_{dl} can be expressed by the following Eq. 1.1

$$\frac{1}{C_{dl}} = \frac{1}{C_H} + \frac{1}{C_{diff}} \dots\dots\dots\dots\dots\dots.1.1$$

According to the charge storage method, only the electrostatic surface charge plays a vital part in storing energy in EDLCs, which ensures quick energy intake and delivery capability to produce superior power performance. Furthermore, because the electrostatic charge storage mechanism (as shown in Figure 1.3.2.2) eliminates volume expansion associated with charge-discharge processes in batteries, SC electrodes can theoretically survive millions of cycles compared to a few thousand cycles for batteries. SC electrodes can theoretically stay millions of cycles.
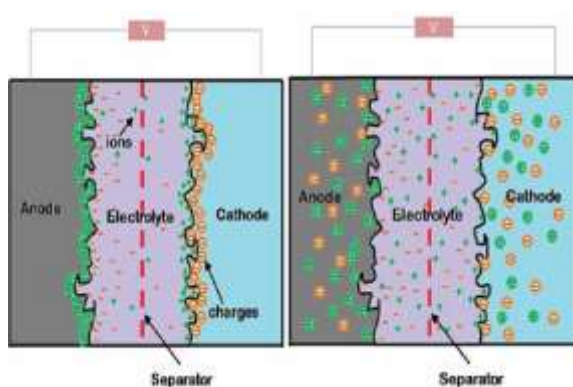
Figure 1.3.2.2 Schematic representation of a porous carbon EDLC in a charged (left) and discharged state (right) [59].

> **Pseudocapacitance**

Pseudocapacitive electrode materials vary from EDLC in those redox processes that occur at or near the surface of the electrode materials to accumulate respective capacitance, comparable to the behavior of batteries. Pseudocapacitance is accompanied by a one-electron-per-charge-unit electron charge transfer between the electrolyte and the electrode. "pseudo" comes from fast faradaic charge transfer processes rather than electrostatic charging. Conway identified several faradaic mechanisms that can result in capacitive electrochemical features: (1) underpotential deposition, (2) redox pseudocapacitance, and (3) intercalation pseudocapacitance [60, 61]. These processes are illustrated in **Figure 1.3.2.3.**
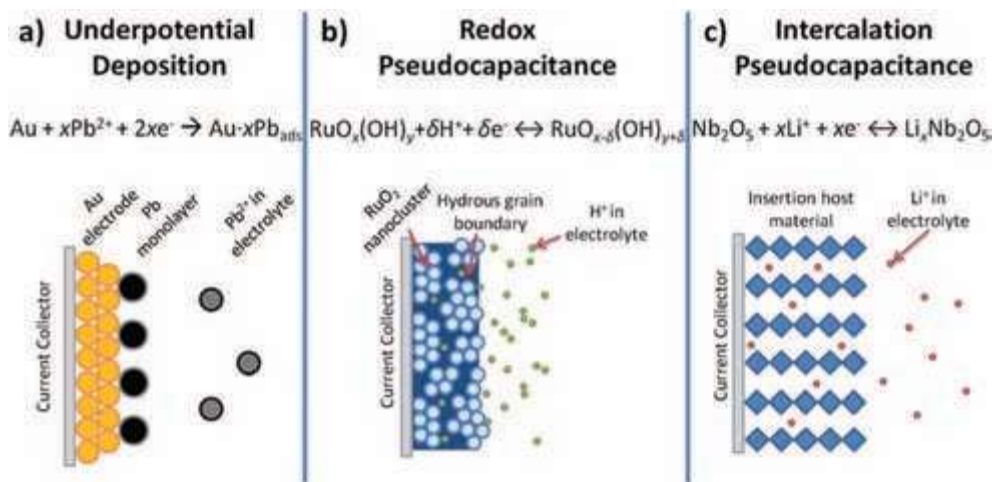
Figure 1.3.2.3 Different types of reversible redox mechanisms that give rise to pseudocapacitance: (a) underpotential deposition, (b) redox pseudocapacitance, and (c) intercalation pseudocapacitance [61].

Underpotential deposition occurs when metal ions form an adsorbed monolayer at a different metal's surface well above their redox potential. Redox pseudocapacitance occurs when ions are electrochemically adsorbed onto the surface or near the surface of a material with a concomitant faradaic charge transfer. Intercalation pseudocapacitance occurs when ions intercalate into the tunnels or layers of a redox-active material accompanied by a faradaic charge transfer with no crystallographic phase change [62, 63]. Pseudocapacitance effects (electron sorption of H or metal atoms, redox reactions of electroactive species) strongly depend on the chemical affinity of carbon materials to the ion's sorbet on the electrode surface [47, 64]. Electrodes with pseudocapacitance are less dependent on the surface area and often deliver higher Csp than traditional carbon-based materials using an EDL charge storage mechanism. Although surface reactions offer higher capacitance and better electrochemical performance, they also cause the failure of electrode stability during cycling.

1.4 Components of supercapacitors
1.4.1 Electrode materials

Based on the electric storage mechanisms and the electrode materials' nature, three main categories of electroactive materials are used in research to fabricate SCs electrodes

- carbon-based EDLC materials
- metal oxides / hydroxides / nitrides / sulfides
- conducting polymers.

The device's performance, cost, and overall stability is the key feature for the assortment of SCs electrodes. Among the carbon-based materials, carbon nanotubes (CNTs), graphene-based structures, which store charges based on non-Faradaic processes relying on their conducting nature and high specific surface area, have been extensively investigated [47, 65]. Ruthenium oxide (RuO_2) has been the focus of research attention for the past few decades as it has three distinct oxidation states below 1.2 V with high C_{sp} in acidic solutions by pseudocapacitive behavior but, till now, more expensive [66]. Metal oxide-MnO_2, Mn_3O_4, Co_3O_4, Fe_2O_3, and NiO, have been investigated as replacements for RuO_2 for less expensiveness and benign properties, but they never reach as high a C_{sp}. Metal hydroxides, nitrides and sulfides are also pseudocapacitive materials, which deliver pseudocapacitance by surface redox reactions [67]. Conducting polymers have also been tested as good SC electrode materials with pseudocapacitive behaviors, and they store charge by bulk processes through doping and non-doping rapidly to high charge densities [68, 69].

➢ Carbon-based EDLC materials- Activated carbon

Due to its ideal charge-discharge behavior, high surface area, cheap cost, outstanding chemical and thermal stability, and strong electrical conductivity, AC is the most extensively utilized active material for at least one of the electrodes in EDLCs, asymmetric SCs, and hybrid SCs. Carbonization in an inert environment is used to make AC from various natural or synthetic carbon-rich organic precursors, followed by physical and/or chemical activation to enhance surface area and pore volume. Gravimetric capacitances of 200-550 F g^{-1} in aqueous electrolytes and 130-230 F g^{-1} in non-aqueous electrolytes have been produced using a variety of AC with specific surface areas (SSA) ranging from 900 to 3500 m^2 [65]. Multiple studies have been done into the possibility of activating and using carbon from agricultural waste as electrode materials in SCs [70, 71]. For instance, Borassus flabellifer flower [72], Willow wood[73], capsicum seed [7], peanut shell[74], cattail wool [75] have been used as sources of precursors for the preparation of AC for SCs. Gao et al. explored rice husk

AC (RHAC) in a symmetric two-electrode configuration successfully exhibited high C_{sp} of 367 F g^{-1} in an aqueous 6 M potassium hydroxide (KOH) electrolyte and 174 F g^{-1} in the organic electrolyte at 5 mV s^{-1}. Yan et al. utilized a waste agricultural by-product, soybean pods, to prepare multi-heteroatom (O, N, and P) self-doping hierarchical structured AC with high surface area via a simple chemical activation strategy, exhibited a high C_{sp} of 321.1 F g^{-1} in aqueous 6M KOH electrolyte [76].

1.4.2 Electrolytes

The electrolyte is also a key component that considerably impacts the SC's performance. Currently, numerous electrolytes have been produced and studied based on the nature of the electrolyte, such as ion type and size, ion concentration and solvent, ion-solvent interaction, ion-electrolyte contact, ion-electrolyte interaction, ion-electrolyte interaction, and the potential window. As seen in **Figure 1.4.2.1,** electrolytes are classified into three types: liquid, solid or semisolid, and redox additive. Aqueous electrolyte, nonaqueous electrolyte, and organic electrolyte are the three types of liquid electrolytes [77, 78]
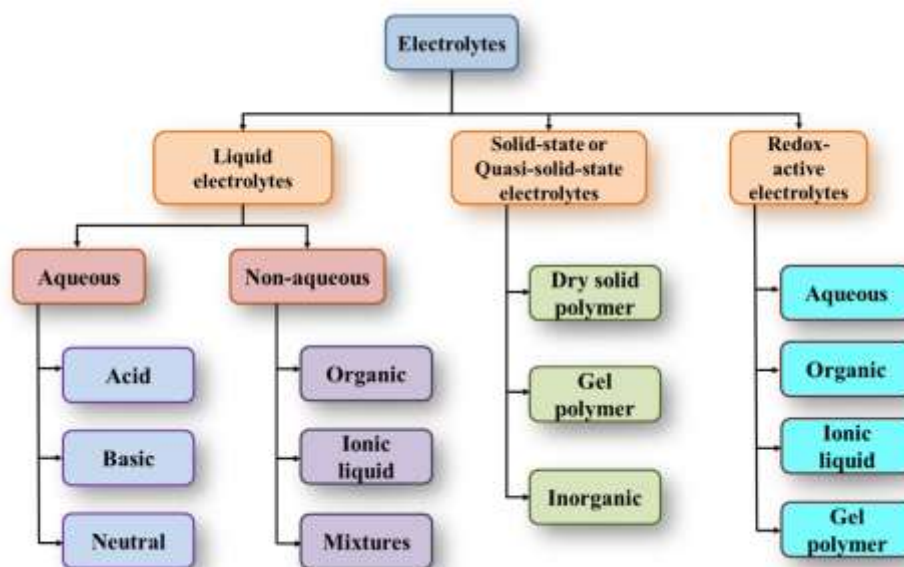
Figure 1.4.2.1 Classification of electrolytes for electrochemical SCs [79].

➢ **Aqueous electrolytes**

Aqueous electrolytes are solutions of acids, alkalis, or neutral salts like KOH and H_2SO_4 that serve as a common and convenient conducting medium in SCs applications [79]. Because of their low cost, strong ionic conductivity, high electrolyte solubility, and less stringent cell-packaging requirements, aqueous electrolytes are often employed in metal-oxide (such as ruthenium oxide) manganese oxides) pseudocapacitors[80]. To increase conductivity (up to 700 mS.cm^{-1} for H_2SO_4) and lower the ESR, relatively high concentrations of aqueous solutions can be created, maximizing the power capability. However, regarding the implications of SC self-discharge, corrosion is a crucial element to consider when choosing the electrolyte and its concentration. Despite the high capacitance values achieved in aqueous systems with AC-based electrodes and metal-oxide based pseudocapacitors, such systems still have low energy densities due to the operating voltage being limited to 1.23 V, which is the electrochemical stability of water [81-83]. The most frequently used aqueous electrolytes are KOH, NaOH, LiOH, Na_2SO_4, H_2SO_4, $(NH_4)_2SO_4$, K_2SO_4, Li_2SO_4, $MgSO_4$, $BaSO_4$, KCl, NaCl etc. with different kinds of electrode materials [21, 22, 34, 84, 85].

➢ **Organic electrolytes**

Organic-based (non-aqueous) electrolytes which generally constitute quaternary ammonium salts solubilized in oxidatively stable organic solvents. Non-aqueous electrolytes are often favored for electrochemical capacitors because they allow for greater working voltages, V, due to the wider decomposition potential limits of this group of electrolyte solutions (up to 2.7 V) [21, 86]. This is a clear advantage over aqueous systems since the stored energy increases with the square of V. The most common solvents used in commercial AC SCs are aprotic solvents (that do not have any dissociable hydrogen), such as acetonitrile (AN) or carbonate-based solvents (propylene carbonate, ethylene carbonate, and so on), which currently offer a wide operating temperature range of -30 °C to +80 °C with a cell voltage of 2.5-2.7 V [87]. Different electrolyte solutions 1 M triethylmethylammonium tetrafluoroborate (TEABF$_4$) in acetonitrile (AN), acetone, g-butyrolactone (GBL), and propylene carbonate (PC) with nanoporous carbon electrodes were used and reported. The most used salts for organic electrolytes are Tetraethylammonium tetrafluoroborate(TEA-

BF$_4$), Methyl Triethyl Ammonium Tetrafluoroborate (TEMABF$_4$), LiPF$_6$ and LiClO$_4$ as reported in the literature [21]. Although their electrochemical stability window is wider than that of aqueous systems, such solvents are generally volatile (hence flammable), necessitating careful and costly thermal control to avoid the risk of explosion due to pressure build-up at high temperatures, endangering the safety of the devices.

> **IL electrolytes**

ILs are commonly used as electrolytes in energy storage devices such as lithium-ion batteries, SCs, and fuel cells [88-91]. IL has unique structures and properties with a large asymmetric organic cation and an inorganic or an organic anion [91]. Therefore, ILs electrolytes attract significant interest as alternative electrolytes for ESs because of their potential advantages, including high thermal, chemical and electrochemical stability, negligible volatility, non-flammability, and no solvation effect. Based on their composition, ILs can be classified as aprotic, protic and zwitterionic types, as shown in Figure 1.4.2.2 [92].
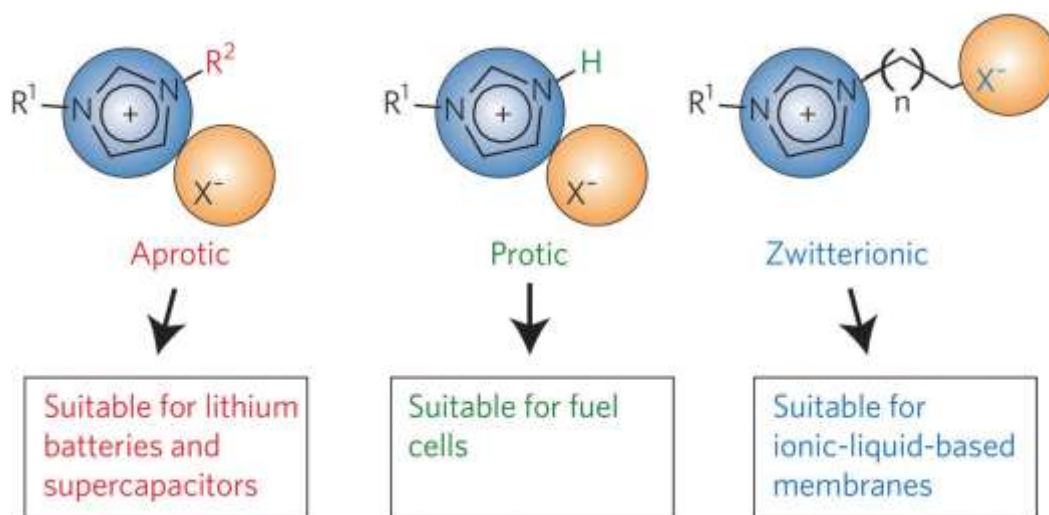
Figure 1.4.2.2 Basic types of ionic liquids: aprotic, protic, and zwitterionic [98]

Commonly used cations   Typical examples

Imidazolium   [EMIM]⁺ $R_1=C_2H_5$ $R_2=H$ $R_3=CH_3$

Pyrrolidinium   PYR$_{14}$ $R_1=CH_3$ $R_2=C_4H_9$

Ammonium   [DEME]⁺ $R_1=CH_3$ $R_2=R_3=C_2H_5$ $R_4=CH_3OC_2H_4$

Sulfonium   [Me$_3$S]⁺ $R_1=R_2=R_3=CH_3$

Phosphonium   P$_{2224}$ $R_1=R_2=R_3=C_2H_5$ $R_4=C_4H_9$

Commonly used anions

Tetrafluoroborate [BF$_4$]⁻   Hexafluorophosphate [PF$_6$]⁻   bis(Fluorosulfonyl)imide [FSI]⁻   bis(Trifluoromethanesulfonyl)imide [TFSI]⁻

Commonly used cations for protic ionic liquids

[Et$_3$NH]⁺   [DIPEA]⁺

Figure 1.4.2.3 Commonly used cations, anions of ILs for ESs, and some typical examples of ILs[98]

For ECSs, ILs employed commonly based on imidazolium, pyrrolidinium, ammonium, sulfonium, phosphonium cations, and so on[93], as shown in Figure **1.4.2.3** Sillars investigated several ILs were investigated as electrolytes for AC-based EDLCs, including 1-ethyl-3-methylimidazolium tetraflouroburate [emim]BF$_4$, 1-ethyl-3-methylimidazolium dicyanamide ([emim][N(CN)$_2$]), 1,2-dimethyl-3-propylimidazolium bis(trifluoromethylsulfonyl) imide ([dmpim][tfsi]), and 1-butyl-3-methylpyrrolidinium tris(pentafluoroethyl) trifluorophosphate ([bmPy] [FAP] and compared them with a 1 M TEABF$_4$/PC organic electrolyte. EDLCs using [bmPy][FAP] IL showed the highest operating voltage of 3.5 V, as depicted in Figure 1.4.2.4 [21, 94].
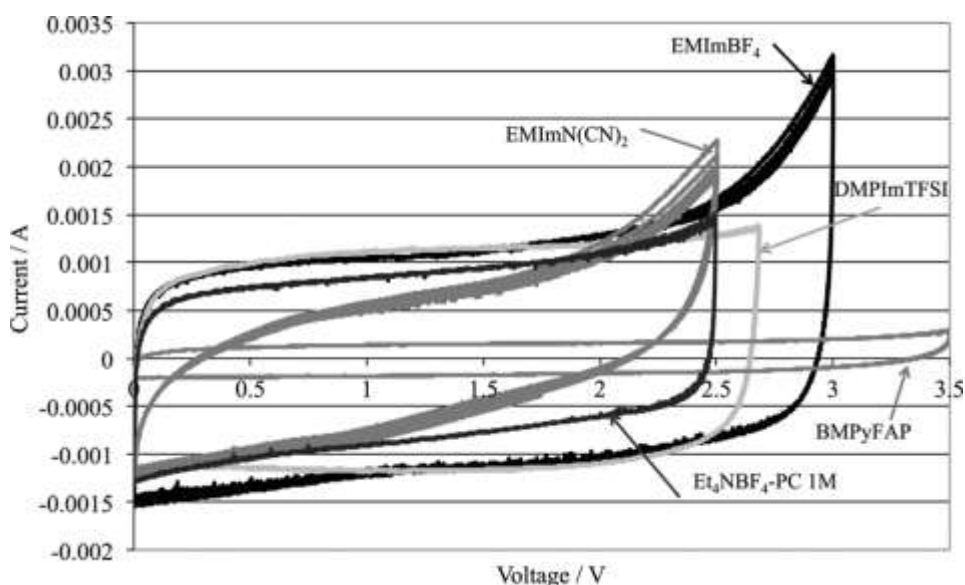
Figure 1.4.2.4 CVs for different ILs at 5 mV s^{-1}. [94]

The hydrophilic– hydrophobic characteristics of ILs are also influenced by their anions [21]. In a two-electrode setup, the electrochemical behavior of graphene sheets (GSs) in five IL electrolytes with the same cation and various anions, including [emim][OAc], [emim][EtSO$_4$], [emim][DCA], [emim]BF$_4$, and [emim][NTf$_2$], was examined. Furthermore, with the same potential window of 2 V, the GS electrodes demonstrated remarkable cycle stability in [emim][DCA], [emim]BF$_4$, and [emim][NTf$_2$]. In terms of E, the GS–[emim]BF$_4$ SC exhibited the largest potential window of 4 V, with a maximum E of 67 Wh kg^{-1} at a current density of 1 Ag^{-1}. The electrochemical characteristics of GSs were greatly altered by the structure of the anions in these ILs [43].

The pictorial represents of ILs of [BMIM]$^+$ cations with different anions, as shown in **Figure 1.4.2.5.** ILs based on imidazolium and pyrrolidinium have attracted interest due to their low viscosity and high ionic conductivity. In general, imidazolium salts were chosen for high ionic conductivity, whereas pyrrolidinium salts were used for a wide range of electrochemical stability. The electrochemical stability window (ESW) of a) imidazolium-based ILs is intrinsically linked to cations, anions, and the amount of carbon atoms in the cation's alkyl side chain. The oxidation and reduction potential limitations of imidazolium-based cations when coupled with various anions and anions when paired with different imidazolium-based cations differ. The redox potentials of the cations and anions do not vary significantly by changing the length of the alkyl side chain. However, due to the different chemistry of the anions, the redox potentials of different anions exhibit a significant variation. The PF$_6$ anion has the most negative reduction potential and the largest oxidation potential and therefore is the most stable anion during the redox reactions. By modifying the length of the alkyl side chain, the redox potentials of the cations and anions do not change considerably. However, due to differences in anion chemistry, the redox potentials of various anions vary significantly. Because the PF$_6^-$ anion has the highest negative reduction potential and the lowest oxidation potential, it is the most stable anion during redox processes.[90-96]

Table 1.1 Physical properties of different ILs

Ionic liquids	Melting Point	Solubility	Appearance
[bmim]Cl	65-70 °C	1.086 g/cm³ Miscible in water	Semi-Solid yellow to orange
[bmim]Br	65-75°C	1.30 g/cm^3 Miscible in water	Semi-solid yellow to orange
[bmim]PF$_6$	-8°C	1.38 g/ cm^3 Insoluble in water	Light yellow transparent liquid

The physical characterization of different ILs described in table 1.4.2.1. PF$_6^-$ anion based ILs interacts with the electrode surface via fluorine atoms and delocalizes the charge on the PF$_6^-$ anions, decreasing the adsorption interaction with the electrode. Also, the more diffused electron density for anions leads to relatively weaker charge variation. Fluorinated ILs (with [PF$_6$]$^-$ anions) have an opposite behavior and charge

transfer direction, which slightly gets electron charge from the electrode surface.[97, 98]
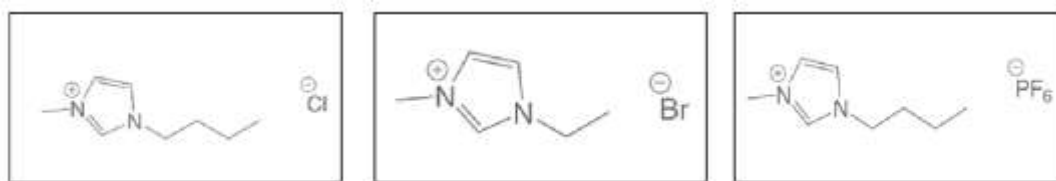
Figure 1.4.2.5 Pictorial representations of three different ILs of [BMIM]$^+$ cations with anions Br$^-$, Cl$^-$ and PF$_6^-$ for ESs [98]

Chloride anions-based ILs have high accessibility and wettability due to highly electronegative atoms, Cl- anions which induce stronger electrostatic interaction with electrode surface, demonstrating more EDLC at low current density. The electron charge transfers from anions to the electrode surface drastically and easily. Whereas bromide anions based ILs provide more diffuse electrons due to larger Br- anions which reduce the interaction of electrolyte and electrode. Another point is that the redox capability influences the electrochemical instability of Br- anions based ILs. [96-98]

1.5 Investigation of electrochemical performance

1.5.1 Electrochemical cell setup- symmetrical two-electrode

A device that generates electrical energy from chemical processes is an electrochemical cell equipped with a current collector, electrodes, and electrolyte. The possible types of electrodes for a standard electrochemical cell setup are fitted with working electrodes (WE), reference electrodes (RE), and counter electrodes (CE). The WE are the electrode under investigation, whereas the CE, or auxiliary electrode, completes the current path in the cell. An electrochemical system with a non-zero current requires a working-counter electrode pair. As its name suggests, the RE is the electrode that serves as an experimental reference point. It serves as a point of reference for potential measurements. As a result, RE should maintain a constant potential during the assessment. Different kinds of cell setups are utilized for performance analysis, namely three electrodes, symmetrical two electrodes, and asymmetrical two-electrode system. Every system has other working principles and points of purpose. We performed our study in a symmetrical two-electrode system. Two-electrode cells are the simplest basic cell structure, yet the data and analysis are usually somewhat involved. Therefore, we

employed a symmetrical electrode system for the electrochemical performance analysis in this work. A symmetric electrode system is one in which two identical electrodes can be used as both the anode and cathode electrodes, as shown in **Figure 1.5.1.1**). In these setups, CE and RE are connected on one side and WE on another side, as designated. In addition, the current-carrying electrodes in a two-electrode configuration can also be utilized to monitor the entire cell voltage.
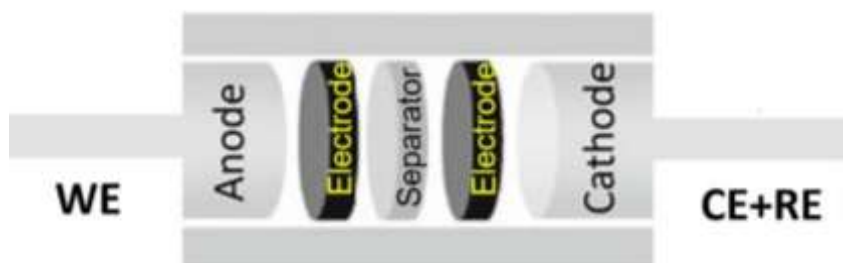
Figure 1.5.1.1 A two-electrode symmetric system, where the electrodes contain the same active material to be studied

1.5.2 Cyclic voltammetry

Cyclic voltammetry (CV) is a powerful and widespread electro-analytical technique commonly employed to investigate molecular specie's reduction and oxidation processes based on the current response of a material as a function of potential. These techniques are also widely used to characterize the performance of various electrical energy storing devices such as SCs.[99, 101] The voltage of the working electrode is scanned for a specified potential (known as a scan window) by executing forward and reverse scans. This process produces a 'cyclic' sweep of potentials that can be repeated, and a cyclic voltammogram, a plot of current vs potential, is created. The initial current response is known as capacitive originating from the electrical double layer (EDL) formed at electrode surface involving diffusion-controlled process as potential allowed to increase.

The anodic peak current and anodic potential are found when the potential approaches a specific value, resulting from the reduction of the active material. Then current falls off when the maximum mass transfer rate has been reached and goes down only to reach equilibrium at some steady value. A similar but opposite peak current may be observed

when potential meets a value resulting in oxidation of the reduced species during its return tour to the initial value [100].

$$R + e^- \leftrightarrow O \quad \text{...............}1.2$$

Faradic current is a response from redox reaction, while the non-Faradic current remains responses usually attributed to EDL. Thus, the capacitive window of a material can be easily identified from the absence or presence of a redox peak in its CV. Scan rate is the rate of change of potential with time. The total current increase is directly proportional to the scan rate, which is rationalized by considering the diffusion layer's size and the time taken to record the scan. The type of the analyte, concentration, scan rates, and experimental circumstances all influence the amplitude of the current response and the form of the voltammograms. The CV may seem somewhat deformed in shape depending on the potential window and materials of interest, suggesting the existence of the faradic process, and charge storage in that potential window area via the faradic process is known as pseudocapacitance. The charge storage and release procedures are capacitive when a CV has a rectangular form. The capacitance calculated from the CV curve is based on the following formula [100]

$$C_{sp} = \frac{\int IdV}{2\vartheta m \nabla V} \quad \text{....................}1.3$$

where "I" is the current (A), "∇V" is the potential difference during the scan (V), 'ϑ' is the scan rate, and "m" is the mass of the active material in gram. "$\int IdV$" is known as the integrated area of the CV curve.

1.5.3 Galvanostatic charge-discharge

Galvanostatic charge-discharge (GCD) is a reliable method to evaluate the electrochemical capacitance of materials under current-controlled conditions. It is known as the chronopotentiometry technique [99-102]. A current pulse is applied to the working electrode, and the resulting potential is measured against a reference electrode as a function of time. The measured potential is abruptly changing due to the internal resistance (*IR*) that resulted from the rapid discharge of reactant from the electrode surface [103]. The following graphs are the current excitation signal and potential response as a function of time.
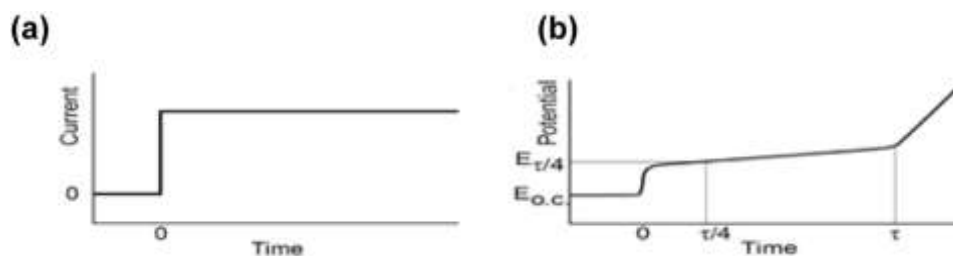
Figure 1.5.3.1 (a) Current excitation and (b) potential response in GCD.

It is possible to identify the nature of the electrode material from the GCD. e.g., the potential response of an ideal capacitive material in GCD shows discharge/ charge time to be ~ 1 and can be easily marked.
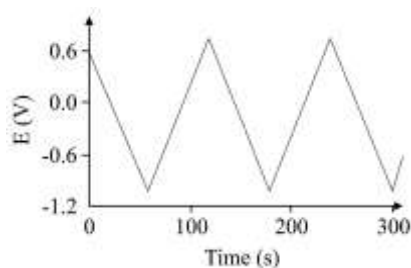
Figure 1.5.3.2 Potential response of an ideal electrochemical capacitor in GCD.

1.5.4 Electrochemical impedance spectroscopy

Electrochemical Impedance Spectroscopy (EIS) is utilized to determine the double-layer capacitance and characterize electrode processes and complex interfaces at various AC frequencies [99, 100]. EIS is a method for establishing a direct link between a real system and an idealized equivalent circuit consisting of discrete electrical components (Resistance, capacitor, and inductor) in series and parallel configurations. Electrochemical capacitors are systems that use either blocking/polarizable electrodes (in the case of EDLC, planar geometries, or high surface area porous electrodes) or electroactive electrode materials (in the case of redox capacitors) [100].
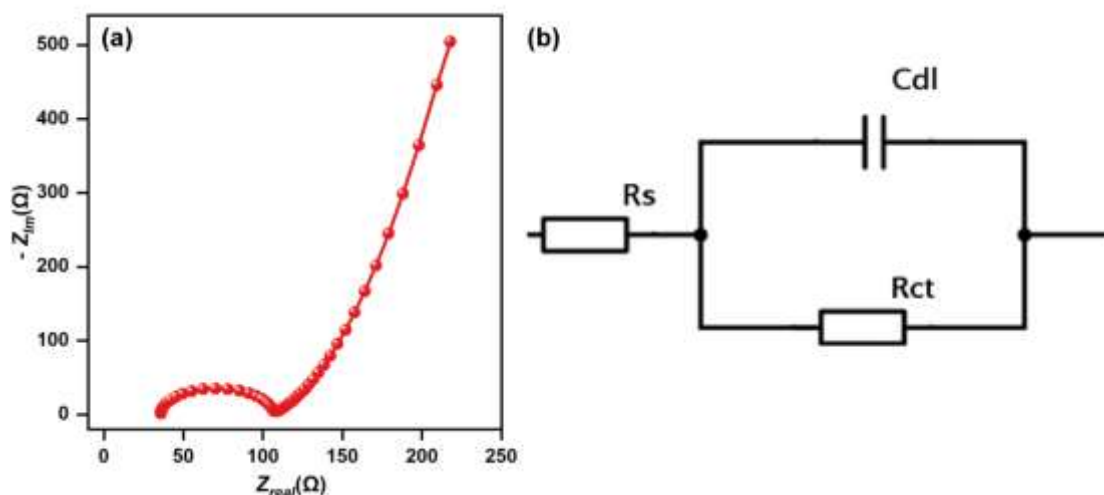
Figure 1.5.4.1(a) A typical Nyquist plot and (b) its equivalent circuit.

Electrochemical Impedance data is represented as the Nyquist plot, which shows how $-Z_{Im}$ varies with Z_{real}, or the Bode plot, which shows how phase angle varies with frequency. Electrochemical processes contain several types of resistance arising from solution (R_s), charge transfer (R_{ct}), EDL (for capacitor), diffusion, etc. Their equivalent circuit, known as the Randles circuit (Figure-.), can be derived from an EIS analysis. It is feasible to determine the type of electroactive material by using EIS. **Figure 1.5.4.1 (b)** shows a typical Nyquist plot and its equivalent circuit

1.5.5 Determination of energy density and power density

The amount of energy stored in a particular mass of a substance, system, or region of space per unit volume is known as energy density [101-105]. The amount of energy contained in the mass of a system or substance is proportional to its E. The fact that an object has a high E does not indicate how rapidly it may be used. P measures power output per unit volume and is defined as the amount of power (time rate of energy transfer) per unit volume. It indicates the rate at which its energy may be released. A high E does not always imply a high P, and it is possible to have a high E and a low P. The E as a function of P is presented in the Ragone plot. Ragone plot compares E of various energy storing devices.

1.6 References

[1]   Zhang, L., Liu, Z., Cui, G., and Chen, L., "Biomass-Derived Materials for Electrochemical Energy Storages," *Prog. Polym. Sci.,* vol. 43, pp. 136-164, 2015.

[2]   Yang, Z., Tian, J., Yin, Z., Cui, C., Qian, W., and Wei, F., "Carbon Nanotube- and Graphene-Based Nanomaterials and Applications in High-Voltage Supercapacitor: A Review," *Carbon,* vol. 141, pp. 467-480, 2019.

[3]   V, A., John, B., and Td, M., "Potassium-Ion Batteries: Key to Future Large-Scale Energy Storage?," *AC Appl. Energy Mater.,* vol. 3, pp. 9478-9492, 2020.

[4]   Makgopa, K., Ejikeme, P. M., Jafta, C. J., Raju, K., Zeiger, M., Presser, V., and Ozoemena, K. I., "A High-Rate Aqueous Symmetric Pseudocapacitor Based on Highly Graphitized Onion-Like Carbon/Birnessite-Type Manganese Oxide Nanohybrids," *J. Mater. Chem. A,* vol. 3, pp. 3480-3490, 2015.

[5]   Ke, Q. and Wang, J., "Graphene-Based Materials for Supercapacitor Electrodes – a Review," *J. Materiomics,* vol. 2, pp. 37-54, 2016.

[6]   Jakubec, P., Bartusek, S., Dvoracek, J. J., Sedajova, V., Kupka, V., and Otyepka, M., "Flax-Derived Carbon: A Highly Durable Electrode Material for Electrochemical Double-Layer Supercapacitors," *Nanomaterials (Basel),* vol. 11, 2021.

[7]   Momodu, D., Sylla, N. F., Mutuma, B., Bello, A., Masikhwa, T., Lindberg, S., Matic, A., and Manyala, N., "Stable Ionic-Liquid-Based Symmetric Supercapacitors from Capsicum Seed-Porous Carbons," *J. Electroanal. Chem.,* vol. 838, pp. 119-128, 2019.

[8]   Reaz, A. H., Barai, H. R., Saha, S., Chowdhury, K., Mojumder, M. N., Firoz, S. H., Chowdhury, A.-N., Joo, S. W., and Roy, C. K., "Self-Doped ACs from Car Exhaust as High-Performance Supercapacitor Electrode Materials for Sustainable Energy Storage System," *J. Electrochem. Soc.,* vol. 168, pp. 080535, 2021.

[9]   Yue, Z., Dunya, H., Ashuri, M., Kucuk, K., Aryal, S., Antonov, S., Alabbad, B., Segre, C. U., and Mandal, B. K., "Synthesis of a Very High Specific Surface Area Active Carbon and Its Electrical Double-Layer Capacitor Properties in Organic Electrolytes," *ChemEngineering,* vol. 4, pp. 43, 2020.

[10]   Zhang, M. *et al.*, "Graphene-Wrapped Mno2 Achieved by Ultrasonic-Assisted Synthesis Applicable for Hybrid High-Energy Supercapacitors," *Vacuum,* vol. 176, pp. 109315, 2020.

[11]   Low, W. H., Khiew, P. S., Lim, S. S., Siong, C. W., and Ezeigwe, E. R., "Recent Development of Mixed Transition Metal Oxide and Graphene/Mixed Transition Metal Oxide Based Hybrid Nanostructures for Advanced Supercapacitors," *J. Alloys Compd.,* vol. 775, pp. 1324-1356, 2019.

[12]   Wang, Q., Yan, J., and Fan, Z., "Carbon Materials for High Volumetric Performance Supercapacitors: Design, Progress, Challenges and Opportunities," *Energy Environ. Sci.,* vol. 9, pp. 729-762, 2016.

[13]   Miao, L., Song, Z., Zhu, D., Li, L., Gan, L., and Liu, M., "Recent Advances in Carbon-Based Supercapacitors," *Mater. Adv.,* vol. 1, pp. 945-966, 2020.

[14]   Jayaraman, T. *et al.*, "Recent Development on Carbon Based Heterostructures for Their Applications in Energy and Environment: A Review," *J. Ind. Eng. Chem.,* vol. 64, pp. 16-59, 2018.

[15]   Jin, Y., Tian, K., Wei, L., Zhang, X., and Guo, X., "Hierarchical Porous Microspheres of Activated Carbon with a High Surface Area from Spores for Electrochemical Double-Layer Capacitors," *J. Mater. Chem. A,* vol. 4, pp. 15968-15979, 2016.

[16]   Liu, Y., Chen, J., Cui, B., Yin, P., and Zhang, C., "Design and Preparation of Biomass-Derived Carbon Materials for Supercapacitors: A Review," *C,* vol. 4, pp.0-14, 2018.

[17]   Momodu, D., Okafor, C., Manyala, N., Bello, A., ZebazeKana, M. G., and Ntsoenzok, E., "Transformation of Plant Biomass Waste into Resourceful Activated Carbon Nanostructures for Mixed-Assembly Type Electrochemical Capacitors," *Waste and Biomass Valorization,* vol. 10, pp. 1741-1753, 2017.

[18]   Yu, G., Hu, L., Vosgueritchian, M., Wang, H., Xie, X., McDonough, J. R., Cui, X., Cui, Y., and Bao, Z., "Solution-Processed Graphene/Mno2 Nanostructured Textiles for High-Performance Electrochemical Capacitors," *Nano Lett.,* vol. 11, pp. 2905-11, 2011.

[19]   Saha, S., Samanta, P., Murmu, N. C., and Kuila, T., "A Review on the Heterostructure Nanomaterials for Supercapacitor Application," *J. Energy Storage,* vol. 17, pp. 181-202, 2018.

[20]   Chen, Z., Jin, L., Hao, W., Ren, W., and Cheng, H. M., "Synthesis and Applications of Three-Dimensional Graphene Network Structures," *Mater. Today Nano,* vol. 5, pp. 100027, 2019.

[21]   Zhong, C., Deng, Y., Hu, W., Qiao, J., Zhang, L., and Zhang, J., "A Review of Electrolyte Materials and Compositions for Electrochemical Supercapacitors," *Chem. Soc. Rev.,* vol. 44, pp. 7484-539, 2015.

[22]   Barzegar, F., Momodu, D. Y., Fashedemi, O. O., Bello, A., Dangbegnon, J. K., and Manyala, N., "Investigation of Different Aqueous Electrolytes on the Electrochemical Performance of Activated Carbon-Based Supercapacitors," *RSC Adv.,* vol. 5, pp. 107482-107487, 2015.

[23]   Dubey, P., Shrivastav, V., Maheshwari, P. H., and Sundriyal, S., "Recent Advances in Biomass Derived Activated Carbon Electrodes for Hybrid Electrochemical Capacitor Applications: Challenges and Opportunities," *Carbon,* vol. 170, pp. 1-29, 2020.

[24]   Miao, L., Duan, H., Wang, Z., Lv, Y., Xiong, W., Zhu, D., Gan, L., Li, L., and Liu, M., "Improving the Pore-Ion Size Compatibility between Poly(Ionic Liquid)-Derived Carbons and High-Voltage Electrolytes for High Energy-Power Supercapacitors," *Chem. Eng. J.,* vol. 382, pp. 122945, 2020.

[25]   Yu, L. and Chen, G. Z., "Ionic Liquid-Based Electrolytes for Supercapacitor and Supercapattery," *Front Chem,* vol. 7, pp. 272, 2019.

[26]   Li, Q., Jiang, J., Li, G., Zhao, W., Zhao, X., and Mu, T., "The Electrochemical Stability of Ionic Liquids and Deep Eutectic Solvents," *Sci. China Chem.,* vol. 59, pp. 571-577, 2016.

[27]   Koh, A. R., Hwang, B., Roh, K. C., and Kim, K., "The Effect of the Ionic Size of Small Quaternary Ammonium Bf(4) Salts on Electrochemical Double Layer Capacitors," *Phys. Chem. Chem. Phys.,* vol. 16, pp. 15146-51, 2014.

[28]   Lazzari, M., Mastragostino, M., Pandolfo, A. G., Ruiz, V., and Soavi, F., "Role of Carbon Porosity and Ion Size in the Development of Ionic Liquid Based Supercapacitors," *J. Electrochem. Soc.,* vol. 158, pp. A22, 2011.

[29]   Kurig, H., Vestli, M., Tõnurist, K., Jänes, A., and Lust, E., "Influence of Room Temperature Ionic Liquid Anion Chemical Composition and Electrical Charge Delocalization on the Supercapacitor Properties," *J. Electrochem. Soc.,* vol. 159, pp. A944-A951, 2012.

[30]   Zhang, H., Cao, G., Yang, Y., and Gu, Z., "Capacitive Performance of an Ultralong Aligned Carbon Nanotube Electrode in an Ionic Liquid at 60°C, " *Carbon,* vol. 46, pp. 30-34, 2008.

[31]   Zhu, Y. *et al.*, "Biomass-Derived Porous Carbon Prepared from Egg White for High-Performance Supercapacitor Electrode Materials, " *ChemistrySelect,* vol. 4, pp. 7358-7365, 2019.

[32]   Zhao, S., Wang, C.-Y., Chen, M.-M., Wang, J., and Shi, Z.-Q., "Potato Starch-Based Activated Carbon Spheres as Electrode Material for Electrochemical Capacitor," *J. Phys. Chem. Solids,* vol. 70, pp. 1256-1260, 2009.

[33]   Pognon, G., Brousse, T., Demarconnay, L., and Bélanger, D., "Performance and Stability of Electrochemical Capacitor Based on Anthraquinone Modified Activated Carbon," *J. Power Sources,* vol. 196, pp. 4117-4122, 2011.

[34]   Vervikishko, D. E., Yanilkin, I. V., Dobele, G. V., Volperts, A., Atamanyuk, I. N., Sametov, A. A., and Shkol'nikov, E. I., "Activated Carbon for Supercapacitor Electrodes with an Aqueous Electrolyte," *High Temp.,* vol. 53, pp. 758-764, 2015.

[35]   Yang, C., Shi, M., Nuli, Y., Song, X., Zhao, L., Liu, J., Zhang, P., and Gao, L., "Interfacial Electrochemical Investigation of 3d Space-Confined Mnfe2o4 for High-Performance Ionic Liquid-Based Supercapacitors," *Electrochim. Acta,* vol. 331, pp. 135386, 2020.

[36]   Yang, P., Xie, J., and Zhong, C., "Biowaste-Derived Three-Dimensional Porous Network Carbon and Bioseparator for High-Performance Asymmetric Supercapacitor," *AC Appl. Energy Mater.,* vol. 1, pp. 616-622, 2018.

[37]   Ahmed, S., Ahmed, A., and Rafat, M., "Supercapacitor Performance of Activated Carbon Derived from Rotten Carrot in Aqueous, Organic and Ionic Liquid Based Electrolytes," *J. Saudi Chem. Soc.,* vol. 22, pp. 993-1002, 2018.

[38]   Galiński, M., Lewandowski, A., and Stępniak, I., "Ionic Liquids as Electrolytes," *Electrochim. Acta,* vol. 51, pp. 5567-5580, 2006.

[39]   Devaki, S. J. and Sasi, R., "Ionic Liquids/Ionic Liquid Crystals for Safe and Sustainable Energy Storage Systems," in *Progress and Developments in Ionic Liquids*, 2017.

[40]   Guo, N., Li, M., Wang, Y., Sun, X., Wang, F., and Yang, R., "Soybean Root-Derived Hierarchical Porous Carbon as Electrode Material for High-

Performance Supercapacitors in Ionic Liquids," *ACS Appl. Mater. Interfaces,* vol. 8, pp. 33626-33634, 2016.

[41] Stoppa, A., Zech, O., Kunz, W., and Buchner, R., "The Conductivity of Imidazolium-Based Ionic Liquids from (−35 to 195) °C. A. Variation of Cation's Alkyl Chain," *J. Chem. Eng. Data,* vol. 55, pp. 1768-1773, 2009.

[42] Muralee Gopi, C. V. V., Vinodh, R., Sambasivam, S., Obaidat, I. M., and Kim, H.-J., "Recent Progress of Advanced Energy Storage Materials for Flexible and Wearable Supercapacitor: From Design and Development to Applications," *J. Energy Storage,* vol. 27, pp. 101035 2020.

[43] Huang, P.-L., Luo, X.-F., Peng, Y.-Y., Pu, N.-W., Ger, M.-D., Yang, C.-H., Wu, T.-Y., and Chang, J.-K., "Ionic Liquid Electrolytes with Various Constituent Ions for Graphene-Based Supercapacitors," *Electrochim. Acta,* vol. 161, pp. 371-377, 2015.

[44] Zhang, S. and Pan, N., "Supercapacitors Performance Evaluation," *Adv. Energy Mater.,* vol. 5, pp. 1401401, 2015.

[45] Zhang, H., Gu, J., Tong, J., Hu, Y., Guan, B., Hu, B., Zhao, J., and Wang, C., "Hierarchical Porous MnO_2 /CeO_2 with High Performance for Supercapacitor Electrodes," *Chem. Eng. J.,* vol. 286, pp. 139-149, 2016.

[46] Raza, W., Ali, F., Raza, N., Luo, Y., Kim, K.-H., Yang, J., Kumar, S., Mehmood, A., and Kwon, E. E., "Recent Advancements in Supercapacitor Technology," *Nano Energy,* vol. 52, pp. 441-473, 2018.

[47] Poonam, Sharma, K., Arora, A., and Tripathi, S. K., "Review of Supercapacitors: Materials and Devices," *J. Energy Storage,* vol. 21, pp. 801-825, 2019.

[48] Wong, S. I., Sunarso, J., Wong, B. T., Lin, H., Yu, A., and Jia, B., "Towards Enhanced Energy Density of Graphene-Based Supercapacitors: Current Status, Approaches, and Future Directions," *J. Power Sources,* vol. 396, pp. 182-206, 2018.

[49] Borah, R., Hughson, F. R., Johnston, J., and Nann, T., "On Battery Materials and Methods," *Mater. Today Adv.,* vol. 6, pp. 100046 , 2020.

[50] Phadke, S., Amara, S., and Anouti, M., "Gas Evolution in Activated-Carbon-Based Supercapacitors with Protic Deep Eutectic Solvent as Electrolyte," *Chemphyschem,* vol. 18, pp. 2364-2373, 2017.

[51]   Haldorai, Y., Giribabu, K., Hwang, S.-K., Kwak, C. H., Huh, Y. S., and Han, Y.-K., "Facile Synthesis of A-MnO$_2$ Nanorod/Graphene Nanocomposite Paper Electrodes Using a 3D Precursor for Supercapacitors and Sensing Platform to Detect 4-Nitrophenol," *Electrochim. Acta,* vol. 222, pp. 717-727, 2016.

[52]   Ma, W. *et al.*, "Influence of Phosphorus Doping on Surface Chemistry and Capacitive Behaviors of Porous Carbon Electrode," *Electrochim. Acta,* vol. 266, pp. 420-430, 2018.

[53]   Muzaffar, A., Ahamed, M. B., Deshmukh, K., and Thirumalai, J., "A Review on Recent Advances in Hybrid Supercapacitors: Design, Fabrication and Applications," *Renew. Sust. Energ. Rev.,* vol. 101, pp. 123-145, 2019.

[54]   Nazarian-Samani, M. *et al.*, "Three-Dimensional Graphene-Based Spheres and Crumpled Balls: Micro- and Nano-Structures, Synthesis Strategies, Properties and Applications," *RSC Adv.,* vol. 6, pp. 50941-50967, 2016.

[55]   Wu, S.-L., Orazem, M. E., Tribollet, B., and Vivier, V., "The Impedance Response of Rotating Disk Electrodes," *J. Electroanal. Chem.,* vol. 737, pp. 11-22, 2015.

[56]   Ratajczak, P., Suss, M. E., Kaasik, F., and Béguin, F., "Carbon Electrodes for Capacitive Technologies", *Energy Storage Mater.,* vol. 16, pp. 126-145, 2019.

[57]   Borenstein, A., Hanna, O., Attias, R., Luski, S., Brousse, T., and Aurbach, D., "Carbon-Based Composite Materials for Supercapacitor Electrodes: A Review," *J. Mater. Chem. A,* vol. 5, pp. 12653-12672, 2017.

[58]   Pilon, L., Wang, H., and d'Entremont, A., "Recent Advances in Continuum Modeling of Interfacial and Transport Phenomena in Electric Double Layer Capacitors," *J. Electrochem. Soc.,* vol. 162, pp. A5158-A5178, 2015.

[59]   Wu, X.-L. and Xu, A.-W., "Carbonaceous Hydrogels and Aerogels for Supercapacitors," *J. Mater. Chem. A,* vol. 2, pp. 4852-4864, 2014.

[60]   Conway, B.E. (1999) Electrochemical Supercapacitors: Scientific Fundamentals and Technological Applications. Springer.

[61]   Augustyn, V., Simon, P., and Dunn, B., "Pseudocapacitive Oxide Materials for High-Rate Electrochemical Energy Storage," *Energy Environ. Sci.,* vol. 7, pp. 1597-1614, 2014.

[62]   Tie, D., Huang, S., Wang, J., Ma, J., Zhang, J., and Zhao, Y., "Hybrid Energy Storage Devices: Advanced Electrode Materials and Matching Principles," *Energy Storage Mater.,* vol. 21, pp. 22-40, 2019.

[63]   Mathis, T. S., Kurra, N., Wang, X., Pinto, D., Simon, P., and Gogotsi, Y., "Energy Storage Data Reporting in Perspective—Guidelines for Interpreting the Performance of Electrochemical Energy Storage Systems," *Adv. Energy Mater.,* vol. 9, pp. 1902007 2019.

[64]   Ghosh, S., Barg, S., Jeong, S. M., and Ostrikov, K., "Heteroatom-Doped and Oxygen-Functionalized Nanocarbons for High-Performance Supercapacitors," *Adv. Energy Mater.,* vol. 10, pp. 2001239 2020.

[65]   Liu, C.-F., Liu, Y.-C., Yi, T.-Y., and Hu, C.-C., "Carbon Materials for High-Voltage Supercapacitors," *Carbon,* vol. 145, pp. 529-548, 2019.

[66]   Zhou, L., Li, C., Liu, X., Zhu, Y., Wu, Y., and van Ree, T., "Metal Oxides in Supercapacitors," in *Metal Oxides in Energy Technologies*, 2018, pp. 169-203.

[67]   An, C., Zhang, Y., Guo, H., and Wang, Y., "Metal Oxide-Based Supercapacitors: Progress and Prospectives," *Nanoscale Adv.,* vol. 1, pp. 4644-4658, 2019.

[68]   Fong, K. D., Wang, T., and Smoukov, S. K., "Multidimensional Performance Optimization of Conducting Polymer-Based Supercapacitor Electrodes," *Sustain. Energy Fuels,* vol. 1, pp. 1857-1874, 2017.

[69]   Shown, I., Ganguly, A., Chen, L. C., and Chen, K. H., "Conducting Polymer-Based Flexible Supercapacitor," *Energy Sci. Eng.,* vol. 3, pp. 2-26, 2014.

[70]   Abioye, A. M. and Ani, F. N., "Recent Development in the Production of Activated Carbon Electrodes from Agricultural Waste Biomass for Supercapacitors: A Review," *Renew. Sust. Energ. Rev.,* vol. 52, pp. 1282-1293, 2015.

[71]   Qian, L., Guo, F., Jia, X., Zhan, Y., Zhou, H., Jiang, X., and Tao, C., "Recent Development in the Synthesis of Agricultural and Forestry Biomass-Derived Porous Carbons for Supercapacitor Applications: A Review," *Ionics,* vol. 26, pp. 3705-3723, 2020.

[72]   Maria Sundar Raj, F. R., Jaya, N. V., Boopathi, G., Kalpana, D., and Pandurangan, A., "S-Doped Activated Mesoporous Carbon Derived from the Borassus Flabellifer Flower as Active Electrodes for Supercapacitors," *Mater. Chem. Phys.,* vol. 240, pp. 122151 2020.

[73]   Phiri, J., Dou, J., Vuorinen, T., Gane, P. A. C., and Maloney, T. C., "Highly Porous Willow Wood-Derived Activated Carbon for High-Performance Supercapacitor Electrodes," *ACS Omega,* vol. 4, pp. 18108-18117, 2019.

[74]   Wang, J., "Nitrogen-Phosphorus Co-Doped Porous Carbon Based on Peanut Shell for Surpercapactior," *Int. J. Electrochem. Sci.,* pp. 6259-6271, 2018.

[75]   Su, X.-L., Jiang, S., Zheng, G.-P., Zheng, X.-C., Yang, J.-H., and Liu, Z.-Y., "High-Performance Supercapacitors Based on Porous Activated Carbons from Cattail Wool," *J. Mater. Sci.,* vol. 53, pp. 9191-9205, 2018.

[76]   Liu, Z., Zhu, Z., Dai, J., and Yan, Y., "Waste Biomass Based-Activated Carbons Derived from Soybean Pods as Electrode Materials for High-Performance Supercapacitors," *ChemistrySelect,* vol. 3, pp. 5726-5732, 2018.

[77]   Fei Yao and Lee, D. T. P. a. H., "Carbon-Based Materials for Lithium-Ion Batteries, Electrochemical Capacitors, and Their Hybrid Devices," *ChemSusChem,* vol.8, pp. 2284-2311, 2015.

[78]   Ramachandran, R. and Wang, F., "Electrochemical Capacitor Performance: Influence of Aqueous Electrolytes," in *Supercapacitors - Theoretical and Practical Solutions*, 2018.

[79]   Iqbal, M. Z., Zakar, S., and Haider, S. S., "Role of Aqueous Electrolytes on the Performance of Electrochemical Energy Storage Device," *J. Electroanal. Chem.,* vol. 858, pp. 113793, 2020.

[80]   Xu, S.-W., Zhang, M.-C., Zhang, G.-Q., Liu, J.-H., Liu, X.-Z., Zhang, X., Zhao, D.-D., Xu, C.-L., and Zhao, Y.-Q., "Temperature-Dependent Performance of Carbon-Based Supercapacitors with Water-in-Salt Electrolyte," *J. Power Sources,* vol. 441, pp. 227220 ,2019.

[81]   Ma, N., Kosasang, S., Phattharasupakun, N., and Sawangphruk, M., "Addition of Redox Additive to Ionic Liquid Electrolyte for High-Performance Electrochemical Capacitors of N-Doped Graphene Aerogel," *J. Electrochem. Soc.,* vol. 166, pp. A695-A703, 2019.

[82]   Zhang, L. L. and Zhao, X. S., "Carbon-Based Materials as Supercapacitor Electrodes," *Chem. Soc. Rev.,* vol. 38, pp. 2520-31, 2009.

[83]   Chen, L., Bai, H., Huang, Z., and Li, L., "Mechanism Investigation and Suppression of Self-Discharge in Active Electrolyte Enhanced Supercapacitors," *Energy Environ. Sci.,* vol. 7, pp. 1750-1759, 2014.

[84]   Zhao, C. and Zheng, W., "A Review for Aqueous Electrochemical Supercapacitors," *Front. Energy Res.,* vol. 3, 2015.

[85]   Fic, K., Meller, M., Menzel, J., and Frackowiak, E., "Around the Thermodynamic Limitations of Supercapacitors Operating in Aqueous Electrolytes," *Electrochim. Acta,* vol. 206, pp. 496-503, 2016.

[86]   Shakil, R., Shaikh, M. N., Shah, S. S., Reaz, A. H., Roy, C. K., Chowdhury, A. N., and Aziz, M. A., "Development of a Novel Bio-Based Redox Electrolyte Using Pivalic Acid and Ascorbic Acid for the Activated Carbon-Based Supercapacitor Fabrication," *Asian J. Org. Chem.,* vol. 10, pp. 2220-2230, 2021.

[87]   Pieta, P., Obraztsov, I., D'Souza, F., and Kutner, W., "Composites of Conducting Polymers and Various Carbon Nanostructures for Electrochemical Supercapacitors," *ECS J. Solid State Sci. Technol.,* vol. 2, pp. M3120-M3134, 2013.

[88]   Ray, A. and Saruhan, B., "Application of Ionic Liquids for Batteries and Supercapacitors," *Materials (Basel),* vol. 14, 2021.

[89]   Singh, V. V., Nigam, A. K., Batra, A., Boopathi, M., Singh, B., and Vijayaraghavan, R., "Applications of Ionic Liquids in Electrochemical Sensors and Biosensors," *Int. J. Electrochem.,* vol. 2012, pp. 1-19, 2012.

[90]   Pan, S., Yao, M., Zhang, J., Li, B., Xing, C., Song, X., Su, P., and Zhang, H., "Recognition of Ionic Liquids as High-Voltage Electrolytes for Supercapacitors," *Front Chem,* vol. 8, pp. 261, 2020.

[91]   Yoo, J., "Ionic Liquid for High Voltage Supercapacitor," in *Supercapacitors - Theoretical and Practical Solutions*, 2018.

[92]   Arkhipova, E. A., Ivanov, A. S., Maslakov, K. I., and Savilov, S. V., "Nitrogen-Doped Mesoporous Graphene Nanoflakes for High Performance Ionic Liquid Supercapacitors," *Electrochim. Acta,* vol. 353, pp. 136463 2020.

[93]   Krummacher, J., Schütter, C., Hess, L. H., and Balducci, A., "Non-Aqueous Electrolytes for Electrochemical Capacitors," *Curr. Opin. Electrochem.,* vol. 9, pp. 64-69, 2018.

[94]   Sillars, F. B., Fletcher, S. I., Mirzaeian, M., and Hall, P. J., "Variation of Electrochemical Capacitor Performance with Room Temperature Ionic Liquid Electrolyte Viscosity and Ion Size," *Phys. Chem. Chem. Phys.,* vol. 14, pp. 6094-100, 2012.

[95]   Kazemiabnavi, S., Zhang, Z., Thornton, K., and Banerjee, S., "Electrochemical Stability Window of Imidazolium-Based Ionic Liquids as Electrolytes for Lithium Batteries," *J. Phys. Chem. B,* vol. 120, pp. 5691-702, 2016.

[96]   Hayyan, M., Mjalli, F. S., Hashim, M. A., AlNashef, I. M., and Mei, T. X., "Investigating the Electrochemical Windows of Ionic Liquids," *J. Ind. Eng. Chem.,* vol. 19, pp. 106-112, 2013.

[97]   Wei, C., Jiang, K., Fang, T., and Liu, X., "Effects of Anions and Alkyl Chain Length of Imidazolium-Based Ionic Liquids at the Au (111) Surface on Interfacial Structure: A First-Principles Study," *Green Chemical Engineering,* vol. 2, pp. 402-411, 2021.

[98]   Zhong, C., Deng, Y., Hu, W., Qiao, J., Zhang, L., and Zhang, J., "A Review of Electrolyte Materials and Compositions for Electrochemical Supercapacitors," *Chem. Soc. Rev.,* vol. 44, pp. 7484-539, 2015

[99]   Wang, J. (2000) *Analytical Electrochemistry*. 2nd Edition, Wiley-VCH, New York.

[100]   A. Bard, L. F., David Harris, E. S., Charity Robey,Eugene Aiello, Ed. (2000) *Electrochemical Methods - Fundamentals and Applications*, 2nd Edition , JOHN WILEY & SONS, INC., USA.

[101]   Wang, H., Gao, Q., and Hu, J., "Asymmetric Capacitor Based on Superior Porous Ni–Zn–Co Oxide/Hydroxide and Carbon Electrodes," *J. Power Sources,* vol. 195, pp. 3017-3024, 2010.

[102]   Choudhary, Y. S., Jothi, L., and Nageswaran, G., "Electrochemical Characterization," in *Spectroscopic Methods for Nanomaterials Characterization*, 2017, pp. 19-54.

[103]   Islam, T. *et al.*, "High Yield Activated Porous Coal Carbon Nanosheets from Boropukuria Coal Mine as Supercapacitor Material: Investigation of the Charge Storing Mechanism at the Interfacial Region," *J. Energy Storage,* vol. 32, 2020.

[104]   Zhao, X., Hou, Y., Wang, Y., Yang, L., Zhu, L., Cao, R., and Sha, Z., "Prepared MnO_2 with Different Crystal Forms as Electrode Materials for Supercapacitors: Experimental Research from Hydrothermal Crystallization Process to Electrochemical Performances," *RSC Adv.,* vol. 7, pp. 40286-40294, 2017.

[105]   Chee, W. K., Lim, H. N., Zainal, Z., Huang, N. M., Harrison, I., and Andou, Y., "Flexible Graphene-Based Supercapacitors: A Review," *J. Phys. Chem. C,* vol. 120, pp. 4153-4172, 2016.

Chapter-2

Experimental

2 Experimental

2.1 Materials and instruments

All the chemicals and reagents used in this work were analytical grade and were used without further purification. Deionized (DI) water (Barnstead Nanopure, Thermo Scientific, USA) was used to prepare all aqueous solutions employed in this study unless stated otherwise. The chemicals and reagents used in this work are listed below:

Name of chemicals and reagents	Source
Potassium hydroxide(KOH)	Sigma-Aldrich, Switzerland
Potassium carbonate (K_2CO_3)	Sigma-Aldrich, Switzerland
Hydrochloric Acid (HCl)	RCI Labscan, Thailand
1-Butyl-3-methyl-imidazolium-chloride ([bmim]Cl)	Sigma-Aldrich, Switzerland
1-Butyl-3-methyl-imidazolium-bromide ([bmim]Br)	Sigma-Aldrich, Germany
1-Butyl-3-methyl-imidazolium-hexaforophosfate ([bmim]PF_6)	Sigma-Aldrich, Switzerland
polyvinylidene fluoride (PVDF)	Sigma-Aldrich, Germany
N-methyl-2-pyrrolidone (NMP)	Sigma-Aldrich, Germany
Graphite disk plates	OTOOLWORLD, USA

Synthesis and analysis of the samples were performed using the following instruments:

- Digital balance (CX 220, Citizen, USA and GH-252, AND Japan)
- Hotplate with a digital stirrer (CD 162, Stuart, UK)
- Centrifuge machine (Universal 16A, Hettich, Germany)
- Hot air oven (DSO-500D, Digi system, Taiwan)
- Agate mortar (125mm)
- Inert tube furnace (R 50/250/12, Nabertherm, Germany)
- pH meter (3510 pH meters, Jenway, UK)

- Ultrasonic bath (Powersonic 505, Hwashin, S. Korea)
- X-ray diffractometer (PANALYTICAL EMPYREAN X-ray Diffractometer; Empyrean, Malvern Panalytical, UK)
- Field Emission Scanning Electron Microscope (FESEM; JSM-7600F, JEOL, Japan)
- Raman spectroscopy (iHR320, HORIBA, JAPAN)
- Electrochemical workstation (CH660E; CH Instruments, USA)

2.2 Synthesis of activated carbon

AC was prepared by utilizing a simple thermochemical treatment from banana leaves with activating K_2CO_3, as reported by Roy et al. [1]. First, the dried leaves of the banana were collected and subsequently washed with DI water to remove impurities such as dust. Then, they were again dried at 80 °C for 24 h in an electric oven. After this drying, the leaves were pulverized in a blender. The activating agent, K_2CO_3 was mixed with the resulting dried with a mass ratio of 1:2 of banana leaves and K_2CO_3. The resulting mixture was pretreated at 200 °C, and then subsequently washed carbon was pyrolyzed by first heating it from room temperature to 750 °C at a rate of 10 °C min^{-1} for 5 hours, then leaving it at this temperature for 5 h, and then cooling it at a rate of 5 °C min^{-1} back down to room temperature, all in a tube furnace under an inert N_2 atmosphere. Next, the formed products are decomposed and washed away after treating with 1 M HCl and water. Finally, the samples were further dried in an electric oven at 80 °C for 12 h to obtain the AC.

2.3 Characterization of activated carbon

2.3.1 Surface morphology by FESEM

FESEM is a robust advanced tool for material characterization that reveals the external morphology and orientation of the components that comprise the sample [2]. FESEM analysis uses a focused electron beam to obtain complex, high magnification images of a sample's surface topography with a broad depth of field due to the narrow electron beam, giving them a three-dimensional appearance essential for studying sample surface structure [3]. The signals produced by a FESEM come from the electron beam's interaction with atoms at varying depths within the sample. A Field Emission Gun (FEG) is utilized as an electron emitter gun instead of a Thermionic Emission Gun (TEG) in a standard FESEM procedure. Secondary electrons are the most useful for

illustrating morphology and topography on materials, whereas backscattered electrons are the most useful for demonstrating compositional differences in multiphase samples. Most of the time, data is gathered across a specific region of the material's surface, and a 2-dimensional black-and-white picture is created to show spatial differences in these attributes. Areas spanning 1 cm to 5 microns are scanned in a scanning mode (magnification ranging from 20X to approximately 500000X, the spatial resolution of 50 to 100 nm) in FESEM methods. The system is computer interfaced, so the surface pictures are recorded in a computer file for later usage as a hard copy. The FESEM systems employed in this work are depicted in Figure 2.3.1.1 of the JSM-7600F (FE-SEM, Tokyo, Japan) system equipped in the Department of Glass and Ceramic Engineering, Bangladesh University of Engineering and Technology (BUET).

Figure 2.3.1.1 A photo of SEM JSM-7600F.

The surface morphology of the prepared AC was analyzed with FESEM via secondary electron imaging at an accelerating voltage of 15 kV. The AC powder sample was initially placed on a 1 cm $\times$ 1cm conductive copper tape. The sample was then coated with platinum for around 40 seconds using the ion sputtering process in the coater. Finally, the sample is covered with a 10 nm coating of platinum. The sample loaded strip was then mounted to the main FESEM chamber integrated with the instrument to view the sample surface that evacuated to ~ 10^{-3} to 10^{-4} torr. Various magnification range was used, varying from 5000-to 100,000 times.

2.3.2 Electrochemical characterizations of activated carbon

The electrochemical characterization such as CV and GCD, EIS and cyclic stability of AC was performed in a computer-controlled electrochemical working station (CHI 660E, CH Instruments, USA). For investigating the SC performance of the prepared AC materials, two-electrode symmetrical SCs were fabricated using the sandwich method with an electrolyte socked Whatman 40 filter papers between two identically modified graphite electrodes with a surface area of ~0.4 cm^2. Graphite plates (OTOOLWORLD, USA) were acted as the current collector. A homogeneous coating mixture of 20 mg AC active material (95 wt. %) was prepared with 2 mg PVDF binder (10 wt. %) and 250 µL NMP under sonication for an hour to yield a slurry. A volume of 20 µL of the slurry was drop-cast on the electrode surface with a micropipette, following as reported earlier [1].
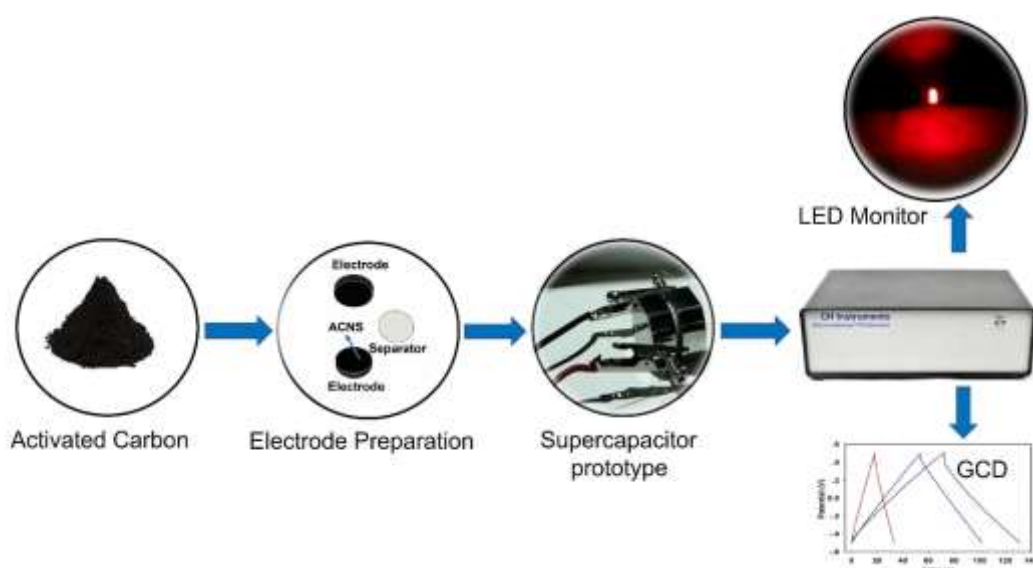
Figure 2.3.2.1 A flowchart of device fabrication for the electrochemical performance analysis of AC

A thin film of the slurry was formed after drying the electrode at 60 °C in a vacuum oven for four hours. The loaded areal density of AC materials over the graphite electrode surface was around 2.0 ~3.0 mg cm^{-2}. The prepared graphite plates modified with the AC slurry were employed in the symmetric SC device as anode and cathode. CV and GCD experiments were carried out using three different pure IL electrolytes: [bmim]Br, [bmim]Cl and [bmim]PF$_6$. The IL electrolytes contained some water content which was not possible to measure. The C_{sp} of a single electrode, E, and P

values of the symmetrical two-electrode system as employed were calculated from the GCD results using the following equations [1, 4].

$$C_{sp} \text{ (F g}^{-1}) = \frac{2I\Delta t}{m\Delta V} \dots\dots\dots\dots\dots\dots \text{ 2.1}$$

$$E \text{ (Wh kg}^{-1}) = \frac{C_{sp}(\Delta V)^2 \times 1000}{8 \times 3600} \dots\dots\dots\dots \text{2.2}$$

$$P \text{ (W kg}^{-1}) = \frac{E \times 3600}{\Delta t} \dots\dots\dots\dots\dots \text{ 2.3}$$

where I, Δt, ΔV, and m are loaded current, discharge time, potential range (cell voltage), and loaded mass of the active material in each working electrode (g). Electrochemical impedance spectroscopic (EIS) experiments for the two-electrode system were conducted at the open-circuit potential within a frequency range of 100 kHz to 0.01 Hz at an AC amplitude of 10 mV. All the electrochemical experiments were carried out at room temperature, 25 $\pm$1 $^{\circ}$C.

2.4 References

[1]   Roy, C. K., Shah, S. S., Reaz, A. H., Sultana, S., Chowdhury, A. N., Firoz, S. H., Zahir, M. H., Ahmed Qasem, M. A., and Aziz, M. A., "Preparation of Hierarchical Porous Activated Carbon from Banana Leaves for High-Performance Supercapacitor: Effect of Type of Electrolytes on Performance," *Chem. Asian J.,* vol. 16, pp. 296-308, 2021.

[2]   Egerton, R. F.,(2005) *Physical Principles of Electron Microscopy*, 1st edition. Springer, Boston, USA.

[3]   Goldstein et *al*.,(2018) *Scanning Electron Microscopy and X-Ray Microanalysis*, Springer, New York, USA.

[4]   Reaz, A. H., Barai, H. R., Saha, S., Chowdhury, K., Mojumder, M. N., Firoz, S. H., Chowdhury, A.-N., Joo, S. W., and Roy, C. K., "Self-Doped Activated Carbons from Car Exhaust as High-Performance Supercapacitor Electrode Materials for Sustainable Energy Storage System," *J. Electrochem. Soc.,* vol. 168, pp. 080535, 2021.

Chapter-3
Results and Discussion

3 Results and discussion

3.1 Synthesis of activated carbon from banana leaves

AC was prepared by utilizing a simple thermochemical treatment from banana leaves with activating K_2CO_3, as reported by Roy et al. [1]. The activating agent, K_2CO_3 was mixed with the resulting dried with a mass ratio of 1:2 of banana leaves and pyrolyzed at a temperature of 750 °C under an inert N_2 atmosphere. The entire process is shown in the schematic diagram of Figure 3.3.1

Figure 3.1.1 A flowchart shows all AC-based materials synthesis pathways

The resulting annealed mixture was collected, washed, and dried; detailed preparation techniques are explained in the experimental section.

3.2 Morphology study by FESEM

The surface morphology of the prepared NAC and AC was investigated by observing the FESEM images, as demonstrated in **Figure 3.2.1 (a) and (b),** respectively. As shown in **Figure 3.2.1 (a),** the surface of the synthesized nanostructured NAC was slightly agglomerated and not homogeneous. In addition, no porous structure appeared for NAC due to buried impurities forming the thick layer of carbon that are barriers to making micropores in the NAC.
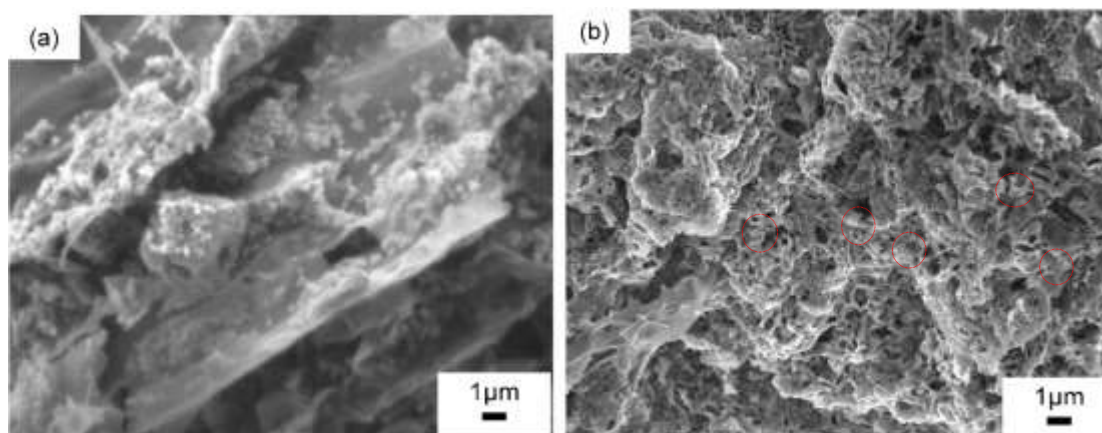
Figure 3.2.1 FESEM images of the carbon materials prepared from banana leaves: (a) NAC and (b) AC

Figure 3.2.1 (b) shows the FESEM of AC. As can be observed in the FESEM image, it shows a high yield of self-supported 3D porous nanostructure with almost homogenous dispersed nanoporous, which may play an important role in its energy storage applications. As a result, the self-supported 3D porous nanostructure of the AC developed in this study should be very attractive for SC applications. It can serve as a template for cyclic stability while also providing a large surface area for EDL development [2-4]. The extremely porous AC is also predicted to have high energy storage capacity since the many pores allow for easy access to many electrolyte ions.

3.3 Investigation of electrochemical performance

All the characterization techniques stated above reveal the structural advantages, including a three-dimensional hierarchical framework, wide pore size distribution, enlarged surface area with enhanced hydrophilicity of the prepared carbon materials, which make them preferable candidates as AC based electrode materials for the SCs with wide variety of electrolytes.

3.3.1 CV and GCD of AC in [bmim]Br electrolyte

To investigate the charge storage mechanism of the AC, CV was performed within the potential range from 0 to 1.0 V at different scan rates of 5, 10, 20, 50 and 100 mV s^{-1} in [bmim]Br electrolyte, is represented in **Figure 3.3.1.1(a).** The CV curve shows the almost symmetric rectangular shape within the potential range, but a redox hump appeared after a potential 0.8 V, which may be attributed to the low electrochemical

stability of [bmim]Br electrolyte as it is so hygroscopic and it contained some water content. Such curves indicate that the charge storage is dominated by both EDL and pseudocapacitive mechanism [5, 6]. Furthermore, it was also observed that the area enclosed by the CV curve increased with the increase of scan rate; the current show an increasing tendency indicating fast ion transportation and good capacitance retention of the prepared sample in wet [bmim]Br. The deviation rectangular shape of the CV curve at higher scan rates and potential may attribute to the short, time-limited movement of electrolyte ions at the electrode surface [7], and redox hump peaks may be caused because of bromide at a higher potential range [8]. The redox reaction that takes place is denoted as follows.

$$2Br^- \Leftrightarrow Br_2 + 2e^- \Leftrightarrow Br_3^-$$

Figure 3.3.1.1 Electrochemical capacitive behaviors of the AC studied using a two-electrode system in wet [bmim]Br electrolyte; (a) CVs at a different scan rate from 5 to 100 mV s^{-1}, (b) GCD curves at different current densities range from 0.5 to 4 A g^{-1}.

The GCD measurements were used to further study the AC sample's electrochemical behavior in wet [bmim]Br liquid. **Figure 3.3.1.1(b)** a show the GCD characteristics of the AC sample in [bmim]Br electrolyte at current densities of 0.5, 1, 2, 3, and 4 A g^{-1}. The potential linear curve over time and symmetry triangle suggested nearly ideal behavior of the electrode material. As the value for current density decreased, the time for GCD increased.

3.3.2 CV and GCD of AC in [bmim]Cl electrolyte

AC was also studied in [bmim]Cl electrolyte within the potential range from 0 to 1.6 V at different scan rates of 5, 10, 20, 50 and 100 mV s^{-1}, is depicted in **Figure 3.3.2.1(a)** The quasi-rectangular rectangular shape of the CV curves without any obvious redox hump to the entire potential range. Wide rectangular CV curves with high current response were observed for all scan rates, defining the EDL nature in [bmim]Cl, indicating its better electronic conductivity due to the easy movement of ions through the hierarchal and porous structure of AC.
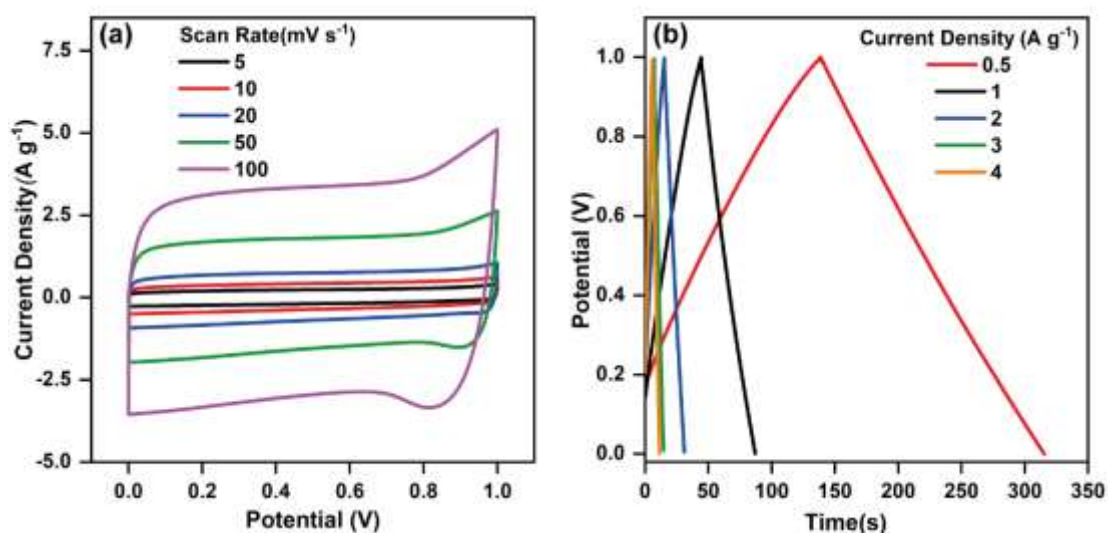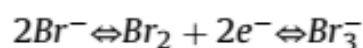

Figure 3.3.2.1 Electrochemical capacitive behaviors of the AC studied using a two-electrode system in [bmim]Cl electrolyte; (a) CVs at a different scan rate from 5 to 100 mV s^{-1}, (b) GCD curves at different current densities range from 0.5 to 4 A g^{-1}.

The capacitance performance of the prepared AC materials was further investigated using the GCD technique at different current densities of 0.5, 1, 2, 3, and 4 A g^{-1} using some water wet [bmim]Cl electrolyte. **Figure 3.3.2.1(b)** illustrates the GCD characteristics of the AC in [bmim]Cl electrolytes. The GCD curves of the AC in [bmim]Cl electrolyte was quasi-symmetrical and relatively triangular in shape, and a longer discharge time of AC in [bmim]Cl electrolyte indicated its higher capacitive performance. Furthermore, the triangular shape of GCD with various current densities was retained event at high current density with high-rate capability and discharge time, indicating high chemical stability of [bmim] Cl electrolyte.

3.3.3 CV and GCD of AC in [bmim]PF$_6$ electrolyte

The CV curves of AC nanocomposite are shown in **Figure 3.3.3.1(a)** within the potential range from 0 to 3.0 V at different scan rates 5 to 100 mV s^{-1} in [bmim]PF$_6$ electrolyte. CV curves of AC are less symmetric with deforming rectangular in shape, indicating the slow charge diffusion of large-fluorinated anions PF$_6$-. However, the curve becomes the more deformed and inclined shape of CVs with increasing scan rate, meaning less ionic mobility and conductivity of [bmim]PF$_6$ electrolyte due to its more hydrophobic and viscous nature. No Redox peak appeared due to the high stability of [bmim]PF6 electrolyte. The phenomenon is attributed to the ohmic resistance for electrolyte motion in porous carbon, in which the storage charge has been recognized to be distributed for the double layer formation mechanism [9]. Additionally, the CV with a lack of symmetry and rectangularity indicates the capacitance is probably due to combined double layer and pseudocapacitance contribution [10]. However, this is due to the electrode material's poor wettability in the electrolyte solution, which results in a smaller surface area available for the formation of an electric double layer, resulting in high resistance to electrolyte ion transport within micropores of porous carbon during charge/discharge processes [11].
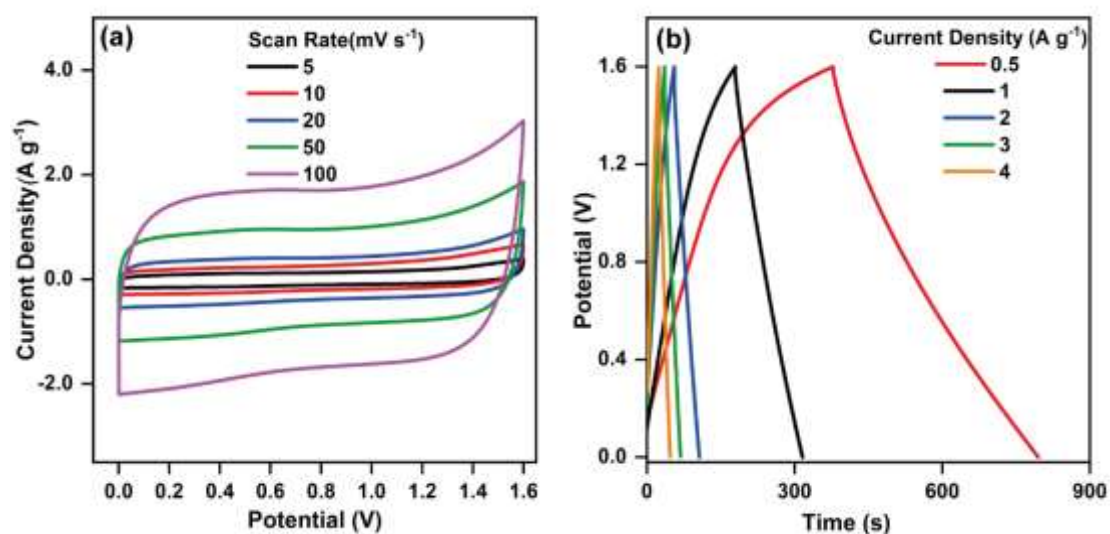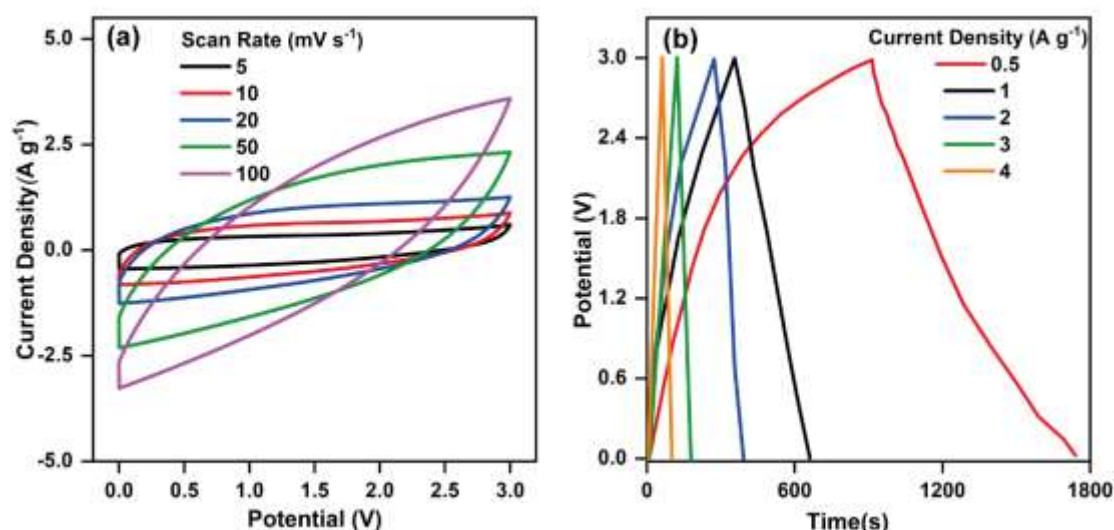

Figure 3.3.3.1 Electrochemical capacitive behaviors of the AC studied using a two-electrode system in [bmim]PF$_6$ electrolyte; (a) CVs at a different scan rate from 5 to 100 mV s^{-1}, (b) GCD curves at different current densities range from 0.5 to 4 A g^{-1}.

Further, GCD at various current densities were studied of AC in [bmim]PF$_6$. **Figure 3.3.3.1(b)** illustrates the GCD curves of AC in [bmim]PF$_6$ electrolytes. The shape of GCD curves was the quasi-symmetrical and relatively triangular shape, and the longer discharge time of AC in [bmim]PF$_6$ electrolyte indicated its higher capacitive performance. The less symmetric GCDs are probably due to the combination of EDL and pseudocapacitance from the slight redox reaction of fluorinated [bmim]PF$_6$ electrolytes[11].

3.4 Comparative studies of electrochemical performances

3.4.1 CV and GCD of AC in [bmim]Br, [bmim]Cl, and [bmim]PF$_6$ electrolytes

Figure 3.4.1.1(a) compares the CV curves of AC in different electrolyte solutions at a fixed scan rate of 20 mV s^{-1} to compare the variation of electrochemical performance. CVs of the AC electrodes were performed between 0 and 1.0 V in [bmim]Br, between 0 and 1.60 V in [bmim]Cl electrolyte, and between 0 and 3.0 V in pure [bmim]PF$_6$ ILs at various scan rates ranging from 5 to100 mV s^{-1}, as shown in **Figure. 3.3.1.1(a), 3.3.2.1(a) and 3.3.3.1(a)**). The AC yielded wide quasi-rectangular CV curves in [bmim]PF$_6$, indicating its EDLC nature in a wide positive potential window range. However, the quasi-rectangular shape of the CV curves was significantly changed at high scan rates for [bmim]PF$_6$ electrolytes, as shown in **Figure 3.4.1.1(a)**. Additionally, the significant rectangular and regular shape of the CV curves were observed even at high scan rates for [bmim]Cl electrolytes, as shown in **Figure 3.3.2.1(a)**. However, the shape of CVs of AC for [bmim]Br electrolyte-maintained rectangularity up to 0 to +0.8 V for forwarding scan and +0.8 to 0 V for reverse scan indicates its dual charge storage capacity in AC electrode, as shown in **Figure 3.3.1.1(a)**. The more rectangular CV curves were attributed to the double-layer formation from the rapid unrestricted motion of electrolyte in the pores of the highly conductive AC [10-13]. This type of EDL formation was facilitated by the mixture of internal and external pore cavities present in the AC, as evident from the FESEM images (**Figure 3.2.1(b)).** Most interestingly, the AC electrode demonstrated good stability over a wide potential range of 0 to 3.0 V in the [bmim]PF$_6$ and up to 1.60 V in [bmim]Cl IL electrolyte without the appearance of any faradic response, but a redox hump appeared for [bmim]Br after 0.8 V. Clearly, the AC can work over a large potential window from 0 to 3.0 V unless the electrolyte

solution supports. The [bmim]Br electrolyte for AC was not suitable outside +1.0 V. In a solvent-free IL medium, the charge storage mainly depends on the layer formation of anions and cations of IL, whereas in an aqueous and protic solvent, it depends on solvated ions. As solvated Cl^- ions are less reactive than solvated Br^- ions in solvent-free IL because the solvent surrounding the chloride in the solvated form of the chloride is a [bmim] cation. $[bmim]^+$ prevents the redox reaction of Cl^- than Br^-. A wide rectangular curve indicates more formation of EDL than Br- and not deformed at a higher scan rate than PF$_6$- anion by applying neat [bmim]Cl. The larger rectangular curve with a higher current response of [bmim]Br is caused by the size difference of the anion because the cations are equal regardless of the change in the anion. The size of ions in the proposed electrolyte is 3.62, 3.90 and 5.10 Å for Br^-, Cl^- and PF_6^-. The CV curve is less rectangular and less symmetric for the [bmim]PF$_6$ containing SC. The deviation from an ideal rectangular shape is due to the high resistive nature of ILs. At a high scan rate, the rectangular shape is deformed because electrolyte ions get little time to penetrate the surface of the electrode. This suggests a very high resistance in the device, which might originate from the higher viscosity of [bmim]PF$_6$ compared to the viscosity of [bmim]Cl, [bmim]Br electrolyte. However, more rectangularity of CV curve for [bmim]Cl electrolyte indicates the electrode/electrolyte interface might be less resistive and exhibits faster kinetic because of the higher ionic conductivity and less viscosity of [bmim]Cl than [bmim]Br and [bmim]PF$_6$.

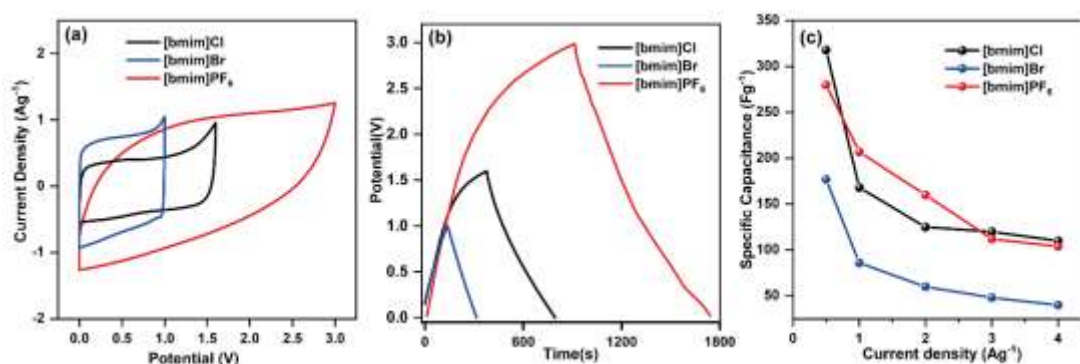**Figure 3.4.1.1** Electrochemical capacitive behaviors of the AC studied using a two-electrode system in three different electrolyte solutions: in [bmim]Br, [bmim]Cl, and [bmim]PF$_6$. Comparison of (a) CVs at a fixed scan rate of 20 mV s^{-1}, (b) GCD curves at a fixed current density of 0.5 A g^{-1}, (c) plots of C_{sp} (F g^{-1}) versus current density for the different electrolyte solutions of AC

The performance of the AC was further confirmed from the results of various GCD experiments carried out with the three different electrolyte solutions, and **Figure 3.4.1.1(b)** shows a comparison of the GCD curves of the AC electrodes with the three different electrolyte solutions each at a fixed current density of 0.5 Ag^{-1}. The slope variation of GCD curves to the time dependence of potential illustrates that the capacitance behavior of the electrodes resulted from the electrochemical adsorption and desorption from the electrode-electrolyte interface. The shape of the GCD curves is in the typical symmetrical or triangular shape of AC for [bmim]Br, [bmim]Cl, and [bmim]PF_6, which indicates no obvious potential drop (*IR* drop), confirming the characteristic EDLC [14]. These curve's most important and interesting feature was the long discharge time associated with the AC. AC electrodes showed the discharge time is 177 , 510 and 841 sec in the [bmim]Br , [bmim]Cl, and [bmim]PF_6 at an applied current density of 0.5 Ag^{-1}. As discharge time indicates the performance of a SC, the GCD results also showed the superior performance of the AC in [bmim]PF_6, but the higher potential is inversely changing the electrode's capacitance.

C_{sp} is an important parameter to consider for evaluating and comparing SC performances. It is often calculated from the GCD profiles of electrode materials of two-electrode systems. The C_{sp} values of the AC electrodes were calculated using Eq (2.1) from the discharging time of GCD curves obtained at different current densities in various electrolytes (**Figures 3.3.1.1(b), 3. 3.2.1(b), and 3.3.3.1(b),** respectively**.** Plots of C_{sp} versus current density are shown in **Figure 3.4.1.1(c).** The maximum C_{sp} values of the AC electrodes in [bmim]Br, [bmim]Cl, and [bmim]PF_6 electrolyte solutions were 177, 318, and 280 Fg^{-1}, respectively. This large difference between their capacitance values clearly reflected the successful execution of the idea of differentiating the effective electrolytes with a highly porous hierarchical carbon for high energy storage capacity. Better capacitances are displayed in the [bmim]Cl electrolyte due to its higher ionic conductivity and lower viscosity. In addition, the smaller anion size of Cl^-, compared to Br^- and PF_6^- anion, may facilitate their reversible adsorption on the AC diffusion of ions from the electrolyte can gain access to almost all available pores of the electrode, leading to a complete insertion reaction responsible for high capacitance, which is probably due to the double-layer capacitance from AC. Free spaces in electrode materials offer more wetted AC by electrolyte to the

electrochemical sites and provide short diffusion path lengths for adsorbing ions with high conductivity, hence better performance

Furthermore, the Csp values obtained for the AC sample were compared with those reported in the literature, as shown in **Table 3.1**. The resulting C_{sp} values of the AC in different electrolytes were comparable with the reported values for AC derived from other biomass sources such as soybean root [15], paulownia flower [16] and sunflower stalk [17]. The C_{sp} values of the currently developed AC were likewise high compared to other AC with IL systems described in the literature [18-20]. For example, Ahmed et al. reported that an AC made from rotting carrots had a C_{sp} of 134 F g^{-1} at a current density of 1 mA cm^{-2} with 1-ethyl-3-methylimidazolium trifluoromethanesulfonate IL medium, which was lower than the value achieved for our AC made from banana leaves [19].

Table 3.1 Comparison of carbon material's C_{sp}, E, and P values derived from different biomass precursors, including banana leaves for SC applications in various electrolytes.

Biowaste	C_{sp} (F g^{-1})	E (Wh kg^{-1})	P (W kg^{-1})	Electrolyte	Ref.
Capsicum seed	153	37	1100	[emim][tfsi]	[18]
Rice husk	147	5	25	6 M KOH	[21]
Peanut shell	224	1	25	2.5 M KNO$_3$	[22]
Sunflower stalk	259	35	989	6 M KOH	[17]
Cauliflower	92	17	29	[emim]BF$_4$	[20]
Orange peel	168	23.3	2334	6 M KOH	[23]
Willow wood	197	23	10000	1 M Na$_2$SO$_4$	[24]
Peanut shell	240	19.3	1007	1 M TEABF$_4$/PC	[25]
Banana leaves	177	6.1	125	[bmim]Br	This Work
	318	28.3	200	[bmim]Cl	
	280	87.5	375	[bmim]PF$_6$	

3.4.2 EIS analysis

The fundamental behavior of electrode materials for SCs is investigated by using EIS [26-28]. The electrical properties of the AC cell were further investigated using EIS in different electrolytes. **Figure 3.4.2.1(a)** shows the Nyquist plot from the EIS analysis of the AC cell in different electrolytes-[bmim]Br, [bmim]Cl, and [bmim]PF_6 and corresponding equivalent circuit in Figure **Figure 3.4.2.1(a)**. The values of the solution resistance (R_s) and charge-transfer resistance (R_{ct}) were evaluated from the extrapolation of the Nyquist plot and fitting data to an equivalent circuit (**Figure 3.4.2.1 (b)**). The values are reported in **Table 3.2**. The low R_s of the electrode material (AC) in [bmim]Br and [bmim]Cl electrolytes were compared to [bmim]PF_6 which reveals the good conductivity of AC in [bmim]Br and [bmim]Cl. Low R_s reveals the viscosity factors for tuning the performance, which is related to the inherent lower conductivity and higher viscosity of [bmim]PF_6 IL systems [29, 30]. The partial semicircle arc observed for AC in [bmim]PF_6 compared to other means reveals that the charge transfer and mass transport is faster across the framework of the porous materials for [bmim]Br and [bmim]Cl that reflects on the R_{ct}. Additionally, in the low-frequency region, a stepper vertical line with a slope near 1 for AC in [bmim]Br and [bmim]Cl indicates the ideal capacitive performance and faster ion transport on the electrode surface compared to [bmim]PF_6.
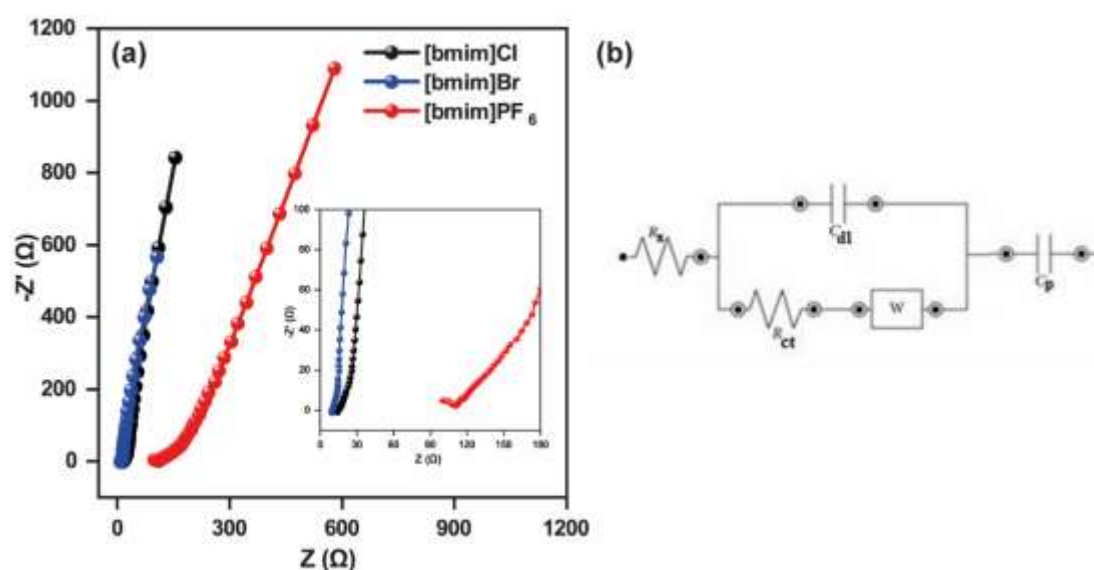

Figure 3.4.2.1 Nyquist plots of AC in the frequency range of 100 kHz to 0.01 Hz at the AC amplitude of 10 mV in room temperature in different ILs electrolytes and (b)

Randle's circuit representing the equivalent circuit where R_s represents electrolyte resistance, C_{dl} stands for the electrical double layer, C_p represents pseudocapacitance, R_{ct} represents the charge transfer resistance, and W represents the Warburg impedance arises from diffusion

Table 3.2 The obtained values of R_S, C_{dl}, C_p, R_{ct} for AC in different IL electrolytes

	R_s (Ω)	R_{ct} (Ω)	$C_{dl}(\mu F)$	$C_p(F)$
[bmim]Br	9.01	1.684	1.1071	0.5019
[bmim]Cl	16.2	1.739	0.93267	0.4081
[bmim]PF$_6$	98.5	57.84	0.02367	0.2083

3.4.3 Determination of energy density and power density

E and P are two important factors to consider when using SCs in practical applications, and they are commonly depicted in a diagram known as a Ragone plot [31]. Equations 2.2 and 2.3 were used to compute the E and P values of AC samples in various electrolyte solutions, which were compared in **Figure 3.4.3.1** This figure also compares the reported E and P values of AC prepared from biomass sources with the AC from other than banana leaves. E values 6.1 , 28.3, and 87.5 Wh kg^{-1} and P values 125, 200, and 375 W kg^{-1} were calculated for the AC [bmim]Br , [bmim]Cl, and [bmim]PF$_6$ electrolytes, respectively. The AC's SC cell with [bmim]PF$_6$ electrolyte had the greatest E and thus the largest P. The high viscosity of IL and the porous nature of AC might respond. The E values are higher than those reported in the literature for other biomass-derived carbon-based SC electrode materials [15-19, 21-23, 32]. In comparison to the AC generated from rice husk [21], peanut shell [22], and cauliflower [20], the P values are likewise high. High E and P levels were acquired from the AC simultaneously. These findings further proved the AC's superiority, as significant E and P values in the same electrode materials are incredibly rare. For most of the previously described AC, a high P-value is related to a low E. High P and E values, like those found in the AC, are required for current SCs to compete with batteries.
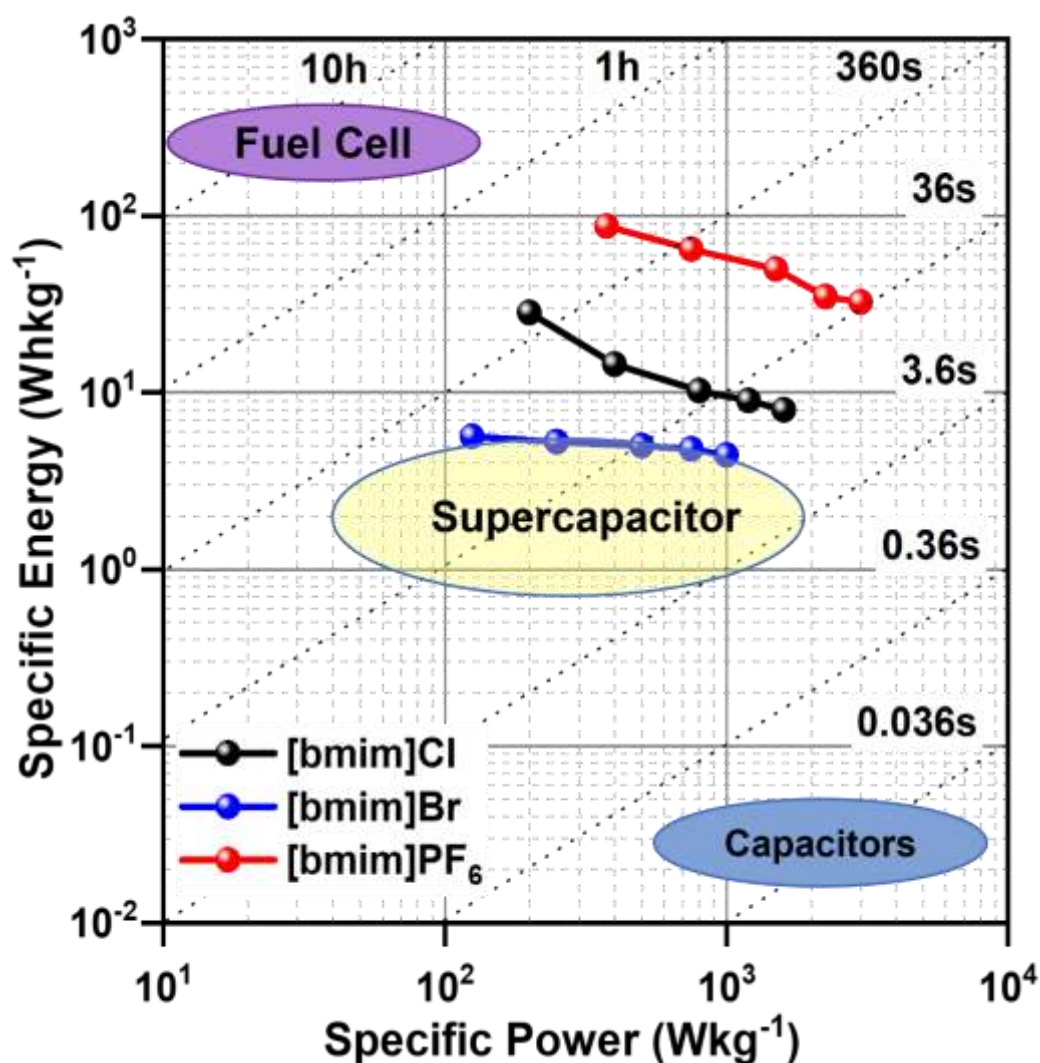
Figure 3.4.3.1 Ragone plot for *E* and *P* of AC in different electrolytes.

3.5 Practical demonstration of prototype device of AC-based symmetric supercapacitor

A mini-prototype device of an AC-based symmetric SC cell was fabricated for a practical demonstration, as illustrated in **Figure 3.5.1(a)**. The experimental design was the same as that used to build the two-electrode device to perform CV and GCD measurements using [bmim]Cl electrolyte. An electrometer was used to charge the device for 160 seconds at 5 V. The gadget was then attached to an LED, and the LED's red glow was utilized to monitor the process. **Figure 3.5.1** shows photographs of the built device and the red LED display used to monitor the SC response.
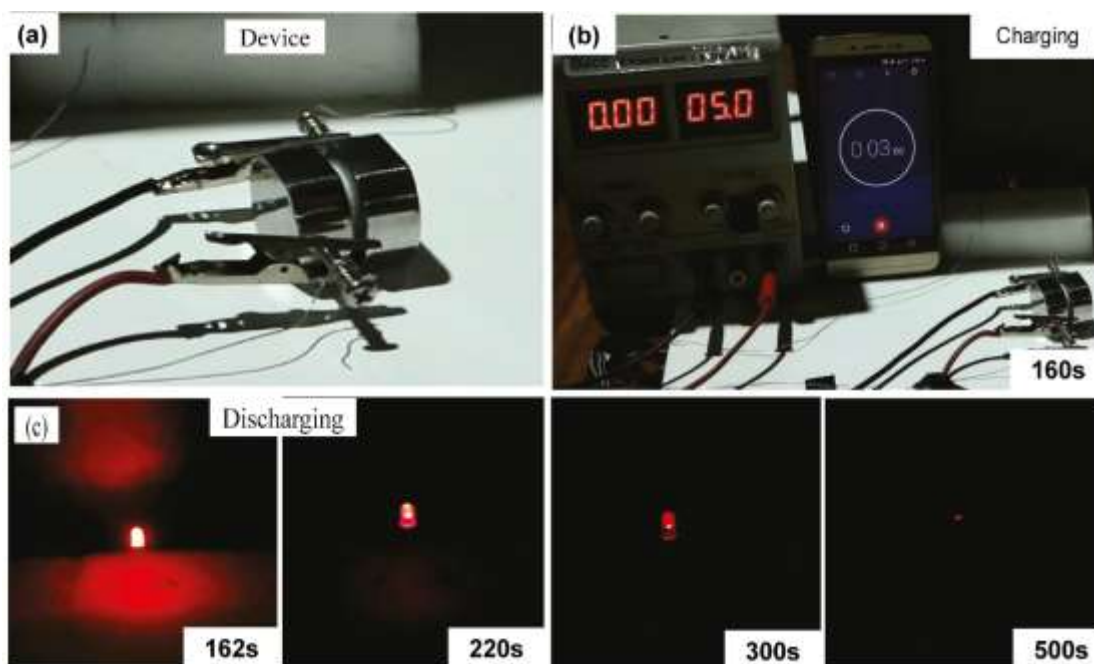
Figure 3.5.1 Photographs are taken to show the performance of a practical AC-containing mini-prototype device SC system using [bmim]Cl. (a) A picture of the device. (b) A photograph of the real device's charging connector. (c) Photos of a system that monitors the discharge process using a red LED glow at different periods as indicated.

3.6 References

[1]   Roy, C. K., Saha, S., and Susan, M. A. B. H.,"Control over Diffusion of Ionic Ferrocene Species in Aqueous Solution Using Surfactant Based Organized Media," *J. Electrochem. Soc.,* vol. 167, pp. 116512, 2020.

[2]   Jin, Y., Tian, K., Wei, L., Zhang, X., and Guo, X., "Hierarchical Porous Microspheres of Activated Carbon with a High Surface Area from Spores for Electrochemical Double-Layer Capacitors," *J. Mater. Chem. A,* vol. 4, pp. 15968-15979, 2016.

[3]   Barzegar, F., Momodu, D. Y., Fashedemi, O. O., Bello, A., Dangbegnon, J. K., and Manyala, N., "Investigation of Different Aqueous Electrolytes on the Electrochemical Performance of Activated Carbon-Based Supercapacitors," *RSC Adv.,* vol. 5, pp. 107482-107487, 2015.

[4]   Fasakin, O., Dangbegnon, J. K., Momodu, D. Y., Madito, M. J., Oyedotun, K. O., Eleruja, M. A., and Manyala, N., "Synthesis and Characterization of Porous

Carbon Derived from Activated Banana Peels with Hierarchical Porosity for Improved Electrochemical Performance," *Electrochim. Acta,* vol. 262, pp. 187-196, 2018.

[5]   Ali, B. A., Metwalli, O. I., Khalil, A. S. G., and Allam, N. K., "Unveiling the Effect of the Structure of Carbon Material on the Charge Storage Mechanism in MoS_2-Based Supercapacitors," *ACS Omega,* vol. 3, pp. 16301-16308, 2018.

[6]   Wu, J., Xia, M., Zhang, X., Chen, Y., Sun, F., Wang, X., Yang, H., and Chen, H., "Hierarchical Porous Carbon Derived from Wood Tar Using Crab as the Template: Performance on Supercapacitor," *J. Power Sources,* vol. 455, pp. 227982, 2020.

[7]   Wu, Z., Li, B., Xue, Y., Li, J., Zhang, Y., and Gao, F., "Fabrication of Defect-Rich MoS_2 ultrathin Nanosheets for Application in Lithium-Ion Batteries and Supercapacitors," *J. Mater. Chem. A* vol. 3, pp. 19445-19454, 2015.

[8]   Pan, S., Yao, M., Zhang, J., Li, B., Xing, C., Song, X., Su, P., and Zhang, H., "Recognition of Ionic Liquids as High-Voltage Electrolytes for Supercapacitors," *Front. Chem.*, vol. 8, pp. 261, 2020.

[9]   Zequine, C. *et al.*, "High-Performance Flexible Supercapacitors Obtained Via Recycled Jute: Bio-Waste to Energy Storage Approach," *Sci Rep,* vol. 7, pp. 1174, 2017.

[10]   Peng, C., Yan, X.-b., Wang, R.-t., Lang, J.-w., Ou, Y.-j., and Xue, Q.-j., "Promising Activated Carbons Derived from Waste Tea-Leaves and Their Application in High Performance Supercapacitors Electrodes," *Electrochim. Acta,* vol. 87, pp. 401-408, 2013.

[11]   Stepniak, I. and Ciszewski, A., "Electric Double Layer Capacitors with Polymer Hydrogel Electrolyte Based on Poly(Acrylamide) and Modified Electrode and Separator Materials," *Electrochim. Acta,* vol. 54, pp. 7396-7400, 2009.

[12]   Bello, A., Manyala, N., Barzegar, F., Khaleed, A. A., Momodu, D. Y., and Dangbegnon, J. K., "Renewable Pine Cone Biomass Derived Carbon Materials for Supercapacitor Application," *RSC Adv.,* vol. 6, pp. 1800-1809, 2016.

[13]   Zhao, S., Liu, T., Shi, D., Zhang, Y., Zeng, W., Li, T., and Miao, B., "Hydrothermal Synthesis of Urchin-Like MnO_2 Nanostructures and Its Electrochemical Character for Supercapacitor," *Appl. Surf. Sci.,* vol. 351, pp. 862-868, 2015.

[14]   Yu, L., Falco, C., Weber, J., White, R. J., Howe, J. Y., and Titirici, M. M., "Carbohydrate-Derived Hydrothermal Carbons: A Thorough Characterization Study," *Langmuir,* vol. 28, pp. 12373-83, 2012.

[15]   Guo, N., Li, M., Wang, Y., Sun, X., Wang, F., and Yang, R., "Soybean Root-Derived Hierarchical Porous Carbon as Electrode Material for High-Performance Supercapacitors in Ionic Liquids," *ACS Appl. Mater. Interfaces,* vol. 8, pp. 33626-33634, 2016.

[16]   Chang, J., Gao, Z., Wang, X., Wu, D., Xu, F., Wang, X., Guo, Y., and Jiang, K., "Activated Porous Carbon Prepared from Paulownia Flower for High Performance Supercapacitor Electrodes," *Electrochim. Acta,* vol. 157, pp. 290-298, 2015.

[17]   Wang, X., Yun, S., Fang, W., Zhang, C., Liang, X., Lei, Z., and Liu, Z., "Layer-Stacking Activated Carbon Derived from Sunflower Stalk as Electrode Materials for High-Performance Supercapacitors," *ACS Sustain. Chem. Eng.,* vol. 6, pp. 11397-11407, 2018.

[18]   Momodu, D., Sylla, N. F., Mutuma, B., Bello, A., Masikhwa, T., Lindberg, S., Matic, A., and Manyala, N., "Stable Ionic-Liquid-Based Symmetric Supercapacitors from Capsicum Seed-Porous Carbons," *J. Electroanal. Chem.,* vol. 838, pp. 119-128, 2019.

[19]   Ahmed, S., Ahmed, A., and Rafat, M., "Supercapacitor Performance of Activated Carbon Derived from Rotten Carrot in Aqueous, Organic and Ionic Liquid Based Electrolytes," *J. Saudi Chem. Soc.,* vol. 22, pp. 993-1002, 2018.

[20]   Karnan, M., Raj, A. G. K., Subramani, K., Santhoshkumar, S., and Sathish, M., "The Fascinating Supercapacitive Performance of Activated Carbon Electrodes with Enhanced Energy Density in Multifarious Electrolytes," *Sustain. Energy Fuels,* vol. 4, pp. 3029-3041, 2020.

[21]   Teo, E. Y. L., Muniandy, L., Ng, E.-P., Adam, F., Mohamed, A. R., Jose, R., and Chong, K. F., "High Surface Area Activated Carbon from Rice Husk as a High Performance Supercapacitor Electrode," *Electrochim. Acta,* vol. 192, pp. 110-119, 2016.

[22]   Sylla, N. F., Ndiaye, N. M., Ngom, B. D., Momodu, D., Madito, M. J., Mutuma, B. K., and Manyala, N., "Effect of Porosity Enhancing Agents on the Electrochemical Performance of High-Energy Ultracapacitor Electrodes Derived from Peanut Shell Waste," *Sci Rep,* vol. 9, pp. 13673, 2019.

[23] Ahmed, S., Rafat, M., and Ahmed, A., "Nitrogen Doped Activated Carbon Derived from Orange Peel for Supercapacitor Application," *Adv. Nat. Sci.: Nanosci. Nanotechnol.,* vol. 9, pp. 035008, 2018.

[24] Phiri, J., Dou, J., Vuorinen, T., Gane, P. A. C., and Maloney, T. C., "Highly Porous Willow Wood-Derived Activated Carbon for High-Performance Supercapacitor Electrodes," *ACS Omega,* vol. 4, pp. 18108-18117, 2019.

[25] He, Y., Chen, W., Li, X., Zhang, Z., Fu, J., Zhao, C., and Xie, E., "Freestanding Three-Dimensional Graphene/MnO$_2$ Composite Networks as Ultralight and Flexible Supercapacitor Electrodes," *ACS Nano,* vol. 7, pp. 174-82, 2013.

[26] Yan, J. *et al.*, "Electrochemical Properties of Graphene Nanosheet/Carbon Black Composites as Electrodes for Supercapacitors," *Carbon,* vol. 48, pp. 1731-1737, 2010.

[27] Wang, D. W., Li, F., Liu, M., Lu, G. Q., and Cheng, H. M., "3D Aperiodic Hierarchical Porous Graphitic Carbon Material for High-Rate Electrochemical Capacitive Energy Storage," *Angew. Chem. Int. Ed. Engl.,* vol. 47, pp. 373-6, 2008.

[28] Li, X., Xing, W., Zhuo, S., Zhou, J., Li, F., Qiao, S. Z., and Lu, G. Q., "Preparation of Capacitor's Electrode from Sunflower Seed Shell," *Bioresour. Technol.,* vol. 102, pp. 1118-23, 2011.

[29] Zhong, C., Deng, Y., Hu, W., Qiao, J., Zhang, L., and Zhang, J., "A Review of Electrolyte Materials and Compositions for Electrochemical Supercapacitors," *Chem. Soc. Rev.,* vol. 44, pp. 7484-539, 2015.

[30] Barzegar, F., Khaleed, A. A., Ugbo, F. U., Oyeniran, K. O., Momodu, D. Y., Bello, A., Dangbegnon, J. K., and Manyala, N., "Cycling and Floating Performance of Symmetric Supercapacitor Derived from Coconut Shell Biomass," *AIP Adv.,* vol. 6, pp. 115306, 2016.

[31] Zhang, S. and Pan, N., "Supercapacitors Performance Evaluation," *Adv. Energy Mater.,* vol. 5, 2015.

[32] He, X., Li, X., Ma, H., Han, J., Zhang, H., Yu, C., Xiao, N., and Qiu, J., "Zno Template Strategy for the Synthesis of 3D Interconnected Graphene Nanocapsules from Coal Tar Pitch as Supercapacitor Electrode Materials," *J. Power Sources,* vol. 340, pp. 183-191, 2017.

Chapter-4
Conclusions

4 Conclusions

In conclusion, unique AC samples were effectively prepared using simple pyrolysis of banana leaves at 750°C in the presence of activating agents K_2CO_3. The preparation of amorphous graphitic carbon was validated by XRD analysis. The morphological and chemical characterizations revealed that the activation procedure has a considerable impact on the microstructure and surface chemistry of these AC materials. The porous structure was shown to be compatible with IL electrolytes of various anions, which is ideal for supercapacitor applications. The AC can work well up to the potential breakdown window of the electrolyte medium. The C_{sp} values are 177, 318, and 280 Fg^{-1} in [bmim]Br, [bmim]Cl, [bmim]PF$_6$ electrolytes, respectively. The AC also shows the largest potential window of 3 V, the highest specific energy (87 Wh kg^{-1}) and specific power (375 W kg^{-1}) in [bmim]PF$_6$. A mini-prototype device is prepared to demonstrate the practicality of the AC using [bmim]Cl. AC generated from other biomass precursors seldom has this mix of characteristics. Furthermore, our findings suggest that the AC with ILs has promising prospects for basic research and industrial energy storage applications.